

Doctoral Thesis

Study of the Schrödinger functional scheme for the
Möbius domain wall fermion

Yuko Murakami

March, 2018

Abstract

One of the goals of quantum chromodynamics (QCD) is to provide a theoretical explanation of the hadron structure. Hadron physics is sensitive to the energy scale. As an example, asymptotic freedom is observed at the higher energies, that corresponds to the perturbative region while, at lower energies or longer distances, strong interactions become truly strong and perturbative techniques break down. Non-perturbative methods are therefore required to analyze low-energy physics based on QCD. Lattice QCD (LQCD) is the non-perturbative definition of QCD constructed in a discretized space-time with finite lattice spacing. Thus, QCD can be analyzed non-perturbatively via numerical simulations using super-computers.

Chiral symmetry plays an important role in hadron and low energy physics in QCD. Because LQCD simulations are required to treat hadron physics or low-energy QCD physics, chiral symmetry is inevitable in such simulations. In LQCD, we cannot describe a lattice fermion operator with chiral symmetry, which is an important property of the massless Dirac fermion. This problem is resolved by extending the chiral symmetry in continuum field theory to a modified chiral symmetry in lattice field theory. This modified chiral symmetry is termed lattice chiral symmetry, and the lattice fermion that satisfies lattice chiral symmetry is referred to as the lattice chiral fermion. The Möbius domain wall fermion (MDWF) is one possible lattice chiral fermions. It is necessary to renormalize the lattice field theory, as is typically done in continuum theory. Especially, it is preferable to employ non-perturbative renormalizations with LQCD. The Schrödinger functional (SF) scheme is one approach to non-perturbative renormalization, and has been successfully applied to the Wilson-type fermions that do not possess lattice chiral symmetry. Applying the SF scheme to lattice chiral fermions is an important subject for future study, but this construction must be done carefully because a special temporal boundary condition is imposed on the fermion operator in the SF scheme.

Lattice chiral symmetry is related to the Ginsparg-Wilson (GW) relation, so lattice chiral fermions satisfy the GW relation. However the temporal boundary condition in the SF scheme incorporates chiral symmetry. When defining a chiral fermion in the SF scheme, it is not a trivial matter to introduce boundary conditions into the definition of a chiral fermion operator by breaking the GW relation at the boundary but maintaining it in the bulk temporal region. There have been several proposed solutions to this issue, among which the universality argument is a simple field theoretic method based on symmetry. SF schemes have been constructed for the overlap and standard domain wall fermions, both of which are lattice chiral fermions, using this argument.

In this thesis, I demonstrate the construction of an SF scheme for the MDWF and validate this approach by comparing the properties of the lattice operator to those of continuum theory in the SF scheme perturbatively, up to the one-loop level. The universality argument imposes some necessary conditions on the operator for the MDWF in the SF scheme. In the future, I anticipate that this approach will be applied to computations of the renormalization constants for lattice chiral fermions (especially the MDWF) using LQCD non-perturbatively, which will reduce the uncertainty associated with observables in hadron physics.

Contents

1	Introduction	4
2	Schrödinger functional scheme	9
2.1	Definitions	9
2.1.1	The continuum theory	9
2.1.2	Lattice field theory	11
2.2	The relationship between the $\overline{\text{MS}}$ and SF schemes	12
2.2.1	The running coupling constant	12
2.2.2	The step scaling function	13
3	The Möbius domain wall fermion	15
3.1	Lattice Möbius domain wall fermion	16
3.2	The effective four-dimensional operator	18
4	Lattice chiral symmetry in the SF scheme	22
4.1	The universality argument	22
4.2	$O(a)$ improvement	23
5	Set up of the SF scheme with the MDWFs	25
5.1	Construction of the operator	25
5.2	Rearrangements of the Zolotarev sign function approximation	27
5.3	The expression of the fermionic contribution $p_{1,1}$	28
6	Numerical results	31
6.1	Properties of the effective four-dimensional operator of the MDWF	32
6.1.1	Unitarity of the effective four-dimensional operator	32
6.1.2	Lattice chiral symmetry breaking in the SF scheme	32
6.2	Universality check at the tree-level	36
6.2.1	Lowest eigenvalues of the Hermitian operator of the MDWFs	36
6.2.2	Snapshot of the spin components of the MDWF propagator	39
6.2.3	Tuning c_{SF} based on the PCAC relation	46
6.3	Universality at the one-loop level	49
6.3.1	Fitting results	50
6.3.2	The cutoff error for the step scaling function	55

7	Summary and Outlook	57
A	Notations	60
B	Zolotarev sign approximation	61

Chapter 1

Introduction

Theoretical research regarding the quantum mechanics of elementary particles began approximately eighty years ago, with work by Yukawa [1]. The discovery of atomic nuclei, in which neutrons and protons are found, required a new kind of force acting between protons and neutrons to explain the formation of nuclei. This new force was termed the *nuclear force*. In 1934, Yukawa published his mesonic theory, which proposed that the nuclear force results from the exchange of unknown particles between neutrons and protons. This particle, named π -*meson*, was experimentally observed in 1947 and was considered at the time to be a fundamental particle. However, in the 1950s, many other particles associated with interactions between protons and neutrons were discovered experimentally. These results showed that various particles, including protons, neutrons and π -mesons, were not fundamental particles but rather could be considered as composite particles, termed hadrons. On this basis, the nuclear force was generalized as a strong interaction and was proposed that more elementary particles should exist.

Gell-Mann and Zweig proposed a model to classify the many hadrons in 1964 [2, 3] and predicted the existence of quarks as elementary particles and the model is termed *quark model*. In 1969, Bjorken reported the scaling property of the structure functions measured in inelastic electron-nucleon scattering experiments [4]. These scaling properties implied that the constituent particles of nucleons were almost point-like and free, and these constituent particles were termed *partons* by Feynman. These partons were later identified with quarks. As quarks or partons inside a nucleon behave as free particles over short distances according to experimental observations, a theory was developed to describe the dynamics of these particles and to predict their properties, which is now known as *asymptotic freedom*. Yang and Mills proposed a non-Abelian gauge theory based on isospin $SU(2)$ symmetry by localizing the symmetry invariance, in an attempt to describe the nuclear force in 1954 [5]. The renormalizability of the Yang-Mills theory was demonstrated by t'Hooft [6, 7]. In the early 1970's, Gross, Wilczek and Politzer reported that a wide class of non-abelian gauge theories (Yang-Mills theories) possess the property of asymptotic freedom [8, 9] based on renormalization group analysis. They also proposed that Yang-Mills theories, especially $SU(3)$ gauge theory, could explain the strong interactions among nucleons. At present, the $SU(3)$ gauge theory, involving several fermions, is referred to us *quantum chromodynamics (QCD)* and

the vector bosons and fermions with the fundamental representation $SU(3)$ are termed gluons and quarks, respectively. The internal degree of freedom based on $SU(3)$ symmetry is referred to as *color*. A degree of freedom for color is necessary based on the properties and classification of hadrons in the original quark model of Gell-Mann and Zweig. Some issues were associated with this original model; free quarks were not observed experimentally, and there were inconsistencies between Pauli's exclusion rule and the baryon wave function made of quarks, as well as between theoretical predictions and experimental results for the total cross section for $e^+e^- \rightarrow$ hadrons and the $\pi \rightarrow 2\gamma$ decay rate. The degree of freedom for color was subsequently introduced in a model by Han and Nambu in 1965 [10] to resolve some of these problems. As noted, the above work is generally referred to as QCD, and is meant to explain the strong interaction among quarks and gluons.

Asymptotic freedom is an important property of QCD. Theoretically, the running coupling constant depends on the energy scale due to the quantum effect, and this coupling becomes weak at the high-energy scale due to the asymptotic freedom of QCD. These are not only desirable for explaining partons (quarks and gluons) as point-like and free particles observed during deep inelastic scattering experiments, but also for theoretical investigations of QCD using the perturbation theory. In contrast, the running coupling constant increases in the low-energy region, which prevents an analytic investigation of the properties of QCD using perturbation theory. The larger coupling constant at lower energies explains, either partially or qualitatively, why isolated quarks have not been observed, based on the confinement of quarks. However, a rigorous explanation for quark confinement is still missing. Because the perturbation theory of QCD is a systematic expansion based on the interaction strength and works only in the case of weak interactions, it is difficult to explain the properties of hadrons analytically. Therefore, in order to elucidate the properties of hadrons theoretically, a theory that can treat QCD without perturbation is required. In 1974, a lattice gauge field theory was proposed to explain quark confinement by Wilson [11], and was termed *lattice quantum chromodynamics (LQCD)*.

LQCD is defined on a discretized space-time box with a finite degree of freedom, and enables the calculation of physical quantities using the first principle of quantum gauge field theory based on computer simulations. Despite this, there is an important problem associated with the formulation of lattice fermion action in LQCD, such that it is not possible to formulate lattice fermion action while satisfying chiral symmetry [12].

Chiral symmetry is a feature for massless fermions under the chiral transformation. This symmetry plays a very important role in hadron physics. As an example, this phenomenon leads to the nucleon mass and the massless pion. Using an effective model that incorporates chiral symmetry, Nambu and Jona-Lasinio demonstrated that nucleon mass and the existence of massless pions as a consequence of the spontaneous breaking of chiral symmetry [13, 14]. QCD is expected to describe and reproduce the spontaneous breaking of chiral symmetry within its quantum dynamics. However, it is impossible to explain spontaneous symmetry breaking analytically using perturbation theory, since the dynamics are completely non-perturbative. Applying the QCD continuum field theory, it is possible to calculate physical quantities with chiral symmetry. Because we cannot formulate a fermion operator satisfying chiral symmetry on a lattice, it becomes difficult to explain the proper-

ties of hadrons, especially based on spontaneous chiral symmetry breaking, at lower energy values using LQCD simulations. Lattice fermion operators with chiral symmetry have a non-physical mode known as a doubler and it is necessary to select lattice fermion operators without a doubler because the doubler affects the associated calculations. Until the early 2000s, LQCD simulations were typically performed using a lattice fermion operator without chiral symmetry.

In contrast, Ginsparg and Wilson proposed that the Dirac fermion operator for a lattice, D , must satisfy the relationship [15],

$$\gamma_5 D + D \gamma_5 = a D \gamma_5 D, \quad (1.0.1)$$

where a is the lattice cutoff and γ_5 is the Dirac gamma matrix. This relationship is extracted from the renormalization group transformation of chiral symmetry in a lattice field, referred to as the *Ginsparg-Wilson (GW) relation*. Lüscher demonstrated that the GW relation represents an alternative chiral symmetry, termed *lattice chiral symmetry* [16]. Although lattice chiral symmetry is not exactly identical to chiral symmetry, the two agree at the continuum limit.

Lattice fermion operators that satisfy lattice chiral symmetry are termed lattice chiral fermion operators. Several formulations have been developed for lattice chiral fermions, including the domain wall fermion (DWF) [17, 18], overlap fermion [19, 20, 21] and the Möbius domain wall fermion (MDWF) [22, 23]. The computational cost of determining these lattice chiral fermions is greater than that for Wilson-type fermions, and so Monte Carlo simulations using Wilson-type fermions were common until the 2000s, at which point 10 Tflop computers became available for simulations. Consequently, Monte Carlo simulations using lattice chiral fermions are currently employed. The hadron mass spectrum, which does not require renormalization, has been established using LQCD simulations and found to be consistent with experimental values. However, it is necessary to renormalize the operator so as to calculate physical quantities in the case of low-energy QCD, which is dominated by spontaneous symmetry breaking, using LQCD based on first principles calculations.

As is typically the case in any quantum field theory, it is necessary to renormalize any physical operators in lattice gauge theory. Lattice field theory introduces a lattice cutoff to regularize the ultraviolet divergences. Typically, all observables in quantum field theories are computed perturbatively and the ultraviolet divergences appear in Feynman's loop diagrams. Renormalization removes these divergences by redefining bare parameters contained in the Lagrangian to obtain finite parameters at an energy scale. There are several schemes for this replacement, one of which scheme is termed the renormalization scheme. The most widely used perturbative renormalization approaches are the minimal subtraction (MS) and modified minimal subtraction ($\overline{\text{MS}}$) schemes. However, these schemes are not suitable for use with lattice field theory because non-perturbative estimates are required for physical quantities in lattice simulations. Thus a non-perturbative renormalization scheme is inevitable in LQCD.

Although non-perturbative renormalization schemes are very attractive and improve the accuracy of physical observables evaluated lattice QCD simulations, there are two problems in defining non-perturbative renormalization schemes for lattice chiral fermions [24]. Firstly, as noted, the computational cost of simulations involving lattice chiral fermions is extremely

high because the overlap fermion maintains strict lattice chiral symmetry, and so simulations employing the overlap fermion are still limited. The DWF has a lower computational cost than that of the overlap fermion by approximating lattice chiral symmetry. However, even using a reasonable level of approximation, the computational cost of the DWF is still high. Secondly, due to the lack of studies on the non-perturbative renormalization schemes for lattice chiral fermions, an optimal renormalization scheme with a modest computational cost together with tolerable numerical accuracy has not been identified. For the first problem, the MDWF could resolve the problem as the numerical cost is significantly lower than that for the overlap and domain wall fermions while lattice chiral symmetry is maintained numerically at a given approximation level. For the second problem, there are several possible non-perturbative renormalization schemes for the lattice, including (i) the regularization independent momentum subtraction (RI-MOM) scheme [25, 26], (ii) the Schrödinger functional (SF) scheme [27, 28, 29, 30], and (iii) the gradient flow [31, 32, 33, 34, 35, 36] scheme. The SF scheme has been employed successfully with Wilson-type fermions and some studies have been done for lattice chiral fermions. An SF scheme for the DWF has been constructed using an orbifolding method by Taniguchi [37, 38]. Lüscher also constructed an SF scheme for overlap fermion using the universality argument, and Takeda investigated its properties perturbatively [39, 40]. Takeda also constructed an SF scheme for the DWF based on Lüscher's universality argument [41]. In this thesis, I report the construction of an SF scheme for the MDWF that resolves the two issues noted above, because the MDWF results in improved lattice chiral symmetry at a lower computational cost compared to the DWF.

The SF scheme developed by Lüscher et al. in the Hamiltonian formalism of lattice gauge theories [27]. In the scheme, the initial state evolves to a final state at a time, T , in a finite space volume, L^3 , according to the Schrödinger equation for lattice gauge theory. The path integral form for the transition amplitude involves initial and final wave functionals that parametrize the gauge field configurations at the initial and final times. A renormalized coupling can be defined with this amplitude by taking the derivative of the parameters. The renormalization scale is then introduced by the space-time volume size T or L . This definition is completely non-perturbative and can be evaluated with lattice gauge theory. Several renormalized quantities with the Wilson-type fermion have been successfully computed in the SF scheme, such as the running coupling constant, fermion masses and properties of renormalization [29, 30], [42]-[52]. As a result, we can obtain quantities in $\overline{\text{MS}}$ scheme from calculations in the SF scheme at the low-energy region.

It is, however, difficult to apply the SF scheme to lattice chiral fermions since the boundary condition of the SF scheme is incompatible with lattice chiral symmetry. Lüscher proposed a realization of the SF scheme for use with the overlap fermion based on the universality argument in the continuum theory, in Ref. [39].

The MDWF is one possible lattice chiral fermion and generalizes the DWFs by introducing several tunable parameters [22, 23]. Although the action of the MDWF is complicated, it approximates lattice chiral symmetry with a minimal computational cost compared to the standard domain wall or overlap fermion. Thus, MDWF action has become the standard lattice chiral fermion action in recent LQCD simulations. As noted above, the mass spectrum does not require renormalization, whereas renormalization is required for operators or

hadronic matrix elements. Even so, only one non-perturbative renormalization schemes have been reported in the literature. Especially, the RI-MOM scheme has been used for lattice chiral fermions. Thus, the SF scheme for lattice chiral fermions could represent an alternative to the RI-MOM scheme. In this thesis, I report the development of an SF scheme for lattice chiral fermions, especially MDWF fermion. Previous studies have been published in Ref. [53, 54, 55, 56].

The structure of this thesis is as follows. In Chapter 2, I introduce the definition of the SF scheme for both continuum theory and lattice field theory. One of the advantages of the SF scheme is that the relationships between the $\overline{\text{MS}}$ and SF schemes are already known for several renormalization constants because the SF scheme has been well studied. I refer to this relationship between the two schemes in this chapter. In Chapter 3, I introduce the definition of the MDWF and explain the properties of this particle in relation to lattice chiral symmetry. Although the MDWF operator is defined as a five-dimensional lattice Dirac operator, the massless portion of the operator is important in low-energy physics and thus we only require the massless portion. A four-dimensional effective operator for the MDWF is therefore extracted from the five-dimensional operator and is described in Chapter 3. Before proceeding with the construction of the operator in the SF scheme, in Chapter 4, I explain the requirements of the SF scheme when employed with the lattice chiral fermion. Following this, I describe the MDWF with the SF boundary operator in Chapter 5. In Chapter 6, I show the numerical results obtained with the operator introduced in Chapter 5. I also investigate the consistency with the requirements outlined in Chapter 4, and discuss the spectral properties and the propagator at the tree-level, and the beta function and running coupling constant at the one-loop level are numerically studied. In the final chapter, I summarize the thesis and predict future prospects based on the theory I constructed for the MDWF in the SF scheme.

Chapter 2

Schrödinger functional scheme

In this chapter, I introduce the SF scheme and the renormalized coupling in the SF scheme. Throughout this work, I consider the $SU(3)$ gauge theory involving fermions in the fundamental representation of the gauge group. This theory is considered for QCD.

2.1 Definitions

2.1.1 The continuum theory

In this section, I introduce the SF scheme in the continuum theory, defined in a finite space-time box. The transition amplitude from an initial state, $|C\rangle$ to a final state $|C'\rangle$, at a time, T , in a finite spatial box with a volume of L^3 is given by

$$\mathcal{Z}[C', C] = \langle C' | e^{-\mathbf{H}T} | C \rangle, \quad (2.1.1)$$

where \mathbf{H} is the Hamiltonian of the $SU(3)$ gauge theory. These states specify the quantum state of the gauge field and fermionic field. Using Feynman's path integral formulation in Euclidean space-time, the amplitude can be written as

$$\mathcal{Z}[C', C] = \int \mathcal{D}[A] \mathcal{D}[\psi] \mathcal{D}[\bar{\psi}] e^{-S[A, \psi, \bar{\psi}]} \Psi_T[C'; A, \psi, \bar{\psi}]^* \Psi_0[C; A, \psi, \bar{\psi}]. \quad (2.1.2)$$

where A is the gauge field, ψ and $\bar{\psi}$ are the fermion fields, and Ψ_0 and Ψ_T are the wave functionals specifying the initial and final states of $|C\rangle$ and $|C'\rangle$, respectively. $S[A, \psi, \bar{\psi}]$ is the action of the $SU(3)$ gauge theory and has the two contributions

$$S[A, \psi, \bar{\psi}] = S_G[A] + S_F[A, \psi, \bar{\psi}], \quad (2.1.3)$$

where S_G is the gauge action and S_F is the fermion action. In this thesis, I focus on the fermion action and omit the details of S_G . According to the SF definition, the continuum action Eq. (2.1.3) is given in a finite box having temporal and spatial extents of T and L , respectively. S_F is described by

$$S_F[A, \psi, \bar{\psi}] = \int_0^{L^3} \int_0^T dx^3 dx_4 \bar{\psi} (\not{D} + m) \psi, \quad (2.1.4)$$

where $\psi, \bar{\psi}$ is the (anti-) fermion field, \mathcal{D} is the continuum massless Dirac fermion operator and m is a bare mass. In the SF scheme, the time evolution of a quantum state based on the Schrödinger equation specifies the boundary condition in the temporal direction in the path integral. In the case of a fermion field, the Dirichlet boundary condition is imposed in the temporal direction of the field, $\psi(x)$, where the temporal coordinate x_4 is in the range of $[0, T]$:

$$P_+ \psi(x)|_{x_4=0} = 0, \quad P_- \psi(x)|_{x_4=T} = 0, \quad (2.1.5a)$$

$$\bar{\psi}(x) P_-|_{x_4=0} = 0, \quad \bar{\psi}(x) P_+|_{x_4=T} = 0. \quad (2.1.5b)$$

Here, P_{\pm} are the temporal projection operators, $P_{\pm} = \frac{1 \pm \gamma_4}{2}$, and the generalized periodic boundary condition in the spatial directions is employed. This condition is given by

$$\psi(\mathbf{x} + L\hat{j}, x_4) = e^{i\theta_j} \psi(\mathbf{x}, x_4), \quad (2.1.6)$$

where \hat{j} is a unit vector in the j -th direction and $\theta_j (j = 1, 2, 3)$ is a real parameter.

To define the running coupling constant in the SF scheme $\bar{g}_{\text{SF}}^2(L)$, I introduce the effective action of the SF [29] as defined by Eq. (2.1.2),

$$\Gamma[B] = -\ln \mathcal{Z}[C', C]. \quad (2.1.7)$$

Generally, we cannot obtain the analytic form of the induced background field B from C' and C but we can define values of C' and C from the induced background field B , which is the unique minimal action configuration. A form of the induced gauge background field is given by the argument of the instant bound for the gauge field action as follows,

$$B_k(x) = \frac{1}{L} \{x_4 C'_k + (L - x_4) C_k\}, \quad B_4(x) = 0, \quad (2.1.8)$$

where C_k and C'_k are the boundary fields depending on the spatial indices ($k = 1, 2,$ and 3),

$$C_k = \frac{i}{L} \text{diag}(\phi_1, \phi_2, \phi_3), \quad C'_k = \frac{i}{L} \text{diag}(\phi'_1, \phi'_2, \phi'_3). \quad (2.1.9)$$

Here, ϕ_{α} and ϕ'_{α} are set in the *fundamental domain* because of the stability of the classical background field, and depend on the external parameter η [27]. α in $\phi_{\alpha}(\phi'_{\alpha})$ is the number of colors ($\alpha = 1, 2,$ or 3).

The effective action, $\Gamma[B]$, is expanded by the bare coupling constant, g_0 , as

$$\Gamma[B] = g_0^{-2} \Gamma_0[B] + \Gamma_1[B] + g_0^2 \Gamma_2[B] + O(g_0^4). \quad (2.1.10)$$

The derivative of B with respect to η is invariant for a renormalization group transformation. The renormalized coupling constant \bar{g}_{SF}^2 is defined by

$$\frac{1}{\bar{g}_{\text{SF}}^2} \frac{\partial}{\partial \eta} \Gamma_0[B]|_{\eta=0} = \frac{\partial}{\partial \eta} \Gamma[B]|_{\eta=0}, \quad (2.1.11)$$

where $\frac{\partial}{\partial \eta} \Gamma_0[B]|_{\eta=0}$ is a normalization factor. The renormalized coupling constant depends on the box size L and the time extent T .

2.1.2 Lattice field theory

The background field

In lattice field theory, the partition function in Eq. (2.1.2) is redefined as

$$\mathcal{Z}_{\text{Lat}}[C, C'] = \int \prod_{n, \mu} dU_\mu(n) d\psi(n) d\bar{\psi}(n) e^{-S_G[U] - S_F[U, \psi, \bar{\psi}]} \Psi_T[C'; U, \psi, \bar{\psi}]^* \Psi_0[C; U, \psi, \bar{\psi}], \quad (2.1.12)$$

where $U_\mu(n)$ is a link field in the $SU(3)$ group with the lattice sites $n = (n_1, n_2, n_3, n_4)$. The relationship between the link field in the lattice and the induced background field in continuum theory is

$$U_\mu(n) = 1 + iaB_\mu(n) + O(a^2). \quad (2.1.13)$$

The link field should give the minimum configuration for the lattice action in the path integral so as to be consistent with that in continuum theory. The spatial gauge field at $n_4 = 0$ and $n_4 = N_T$ is given by

$$U_k(n)|_{n_4=0} = e^{i\hat{C}_k}, \quad U_k(n)|_{n_4=N_T} = e^{i\hat{C}'_k}. \quad (2.1.14)$$

Here, \hat{C}_k and \hat{C}'_k are the boundary fields in the lattice field [29] (c.f. Eq. (2.1.9)) written as

$$\begin{aligned} \hat{C}_k &= \frac{1}{N_S} \text{diag} \left(\eta - \frac{\pi}{3}, \left(-\frac{1}{2} + \nu \right) \eta, \left(-\frac{1}{2} - \nu \right) \eta + \frac{\pi}{3} \right), \\ \hat{C}'_k &= \frac{1}{N_S} \text{diag} \left(-\eta - \pi, \left(\frac{1}{2} + \nu \right) \eta + \frac{\pi}{3}, \left(\frac{1}{2} - \nu \right) \eta + \frac{2\pi}{3} \right), \end{aligned} \quad (2.1.15)$$

where η and ν are parameters of the classic external field introduced by the fundamental domain in the $SU(3)$ gauge field. A solution of the field equations with the SF boundary condition given in Eq. (2.1.8), and indicates a nonzero chromo-electric field. Hence, the classical background gauge field can be written as

$$U_k(n) = \exp \left[i \frac{1}{N_T} (n_4 \phi'_k + (N_T - n_4) \phi_k) \right], \quad U_4(n) = 1. \quad (2.1.16)$$

The lattice renormalized coupling constant in the SF scheme

From the definition of the renormalized coupling constant in the continuum theory in Eq. (2.1.11), the renormalized SF coupling constant \bar{g}_{SF}^2 is given by,

$$\frac{k}{\bar{g}_{SF}^2} \equiv \left. \frac{\partial \Gamma}{\partial \eta} \right|_{\eta=\nu=0}, \quad (2.1.17a)$$

$$k = \left. \frac{\partial \Gamma_0}{\partial \eta} \right|_{\eta=\nu=0} = 12 \left(\frac{a}{L} \right)^2 [\sin(\gamma) + \sin(2\gamma)], \quad \gamma = \frac{\pi}{3} \left(\frac{a}{L} \right)^2. \quad (2.1.17b)$$

Here, k is a renormalization constant that is dependent on the lattice gauge action. k in Eq. (2.1.17b) is the factor for the Wilson gauge action. The renormalized SF coupling constant can be expanded in asymptotic form in terms of the bare coupling as

$$\bar{g}_{SF}^2 = g_0^2 - \frac{1}{k} \frac{\partial \Gamma_1}{\partial \eta} \Big|_{\eta=\nu=0} g_0^4 + \dots \quad (2.1.18)$$

The coefficient of g_0^4 can be separated into gluon and fermion parts as

$$p_1 \equiv -\frac{1}{k} \frac{\partial \Gamma_1}{\partial \eta} \Big|_{\eta=\nu=0} = p_{1,0} + n_f p_{1,1}, \quad (2.1.19)$$

where n_f is the fermion flavor number, and $p_{1,1}$ is associated with the one-loop beta function and confirmed by LQCD calculation. When $\nu = 0$, the statistical error associated with the running coupling becomes minimal [29]. In this thesis, the boundary field in Eq (2.1.15) is set to $\nu = 0$.

2.2 The relationship between the $\overline{\text{MS}}$ and SF schemes

2.2.1 The running coupling constant

In continuum theory, it has been established that the SF scheme is related to the $\overline{\text{MS}}$ scheme with regard to the running coupling constants [29, 57], written as

$$\bar{g}_{\overline{\text{MS}}}^2(\mu) = \bar{g}_{\text{SF}}^2(\mu) [1 + c_1 \alpha_{\text{SF}}(\mu) + \dots], \quad \mu = 1/L, \quad (2.2.1)$$

$$c_1 = c_{1,0} + n_f c_{1,1}, \quad (2.2.2)$$

$$c_{1,0} = 1.25563(4), \quad c_{1,1} = \begin{cases} 0.039863(2) & \text{for } \theta_j = \pi/5 \\ 0.022504(2) & \text{for } \theta_j = 0 \end{cases}, \quad (2.2.3)$$

where $\alpha_{\text{SF}}(\mu)$ is defined as $\alpha_{\text{SF}}(\mu) = \bar{g}_{\text{SF}}^2(\mu)/4\pi$, $c_{1,0}$ is the gluon part [29] and $c_{1,1}$ is the fermionic part [57]. As a result of the relationship in Eq. (2.2.1), we can obtain physical quantities in the $\overline{\text{MS}}$ scheme from quantities calculated with a finite volume in the SF scheme. In the SF scheme, the renormalization group evolution can be traced non-perturbatively using the step scaling method (which is introduced in the next subsection) in conjugation with the lattice technique. Evolving the running coupling constant from a low energy hadronic scale to a high energy scale where the running coupling is sufficiently small, we can accurately convert the coupling constant in the SF scheme to that in the $\overline{\text{MS}}$ scheme via the perturbative formula in Eq. (2.2.1). Similarly, any observables renormalized in the SF scheme can be converted to those in the $\overline{\text{MS}}$ scheme.

The relationship between the two schemes is independent of the regularization used in the SF scheme. Since we employ lattice regularization in the SF scheme, in which the renormalized coupling constant in the SF scheme is expanded by the lattice bare coupling with the lattice cutoff, we require the renormalized coupling constant in the $\overline{\text{MS}}$ scheme in terms of the lattice bare coupling. These two expressions for each coupling in terms of the lattice bare coupling depend on the details of the lattice action used to regularize the calculations, and this topic is discussed in depth in Section 6.2.

2.2.2 The step scaling function

Each renormalized observable in the SF scheme depends on the renormalization scale introduced by the box size of the finite space-time. The renormalization group evolution of the renormalized quantities can be traced using the step scaling function (SSF) method. The SSF for the running coupling in the SF scheme, $\sigma(s, u)$, is defined by

$$\sigma(s, u) = \bar{g}_{\text{SF}}^2(sL), \quad u = \bar{g}_{\text{SF}}^2(L), \quad (2.2.4)$$

where s is a parameter that specifies the renormalization scale evolution. Eq. (2.2.4) is defined in continuum theory, and is independent of the ultraviolet regularization method. In lattice field theory, Eq. (2.2.4) is evaluated in a finite cutoff non-perturbatively, and is taken to the continuum limit. All quantities in the lattice are calculated at a finite cutoff lattice spacing, “ a ”, and are functions of the bare coupling constant, g_0^2 . In the case of Wilson gauge action, $\beta = 6/g_0^2$ is commonly used as the bare coupling. Because $SU(3)$ gauge theory is an asymptotically free theory, the lattice cutoff is a function of the bare coupling constant. Thus, the SSF of the lattice depends on both a/L and β , where a/L parametrizes the lattice size and β implicitly determines a implicitly. The SSF for LQCD, $\Sigma(s, u, a/L)$, is defined as

$$\Sigma(s, u, a/L) = \bar{g}_{\text{SF}}^2(sL, \beta), \quad u = \bar{g}_{\text{SF}}^2(L, \beta), \quad (2.2.5)$$

in which the lattice cutoff dependence is specified by a/L and β . $\Sigma(s, u, a/L)$ contains lattice artifacts that are defined as

$$\delta(u, a/L) = \frac{\Sigma(s, u, a/L) - \sigma(s, u)}{\sigma(s, u)}. \quad (2.2.6)$$

$\delta(u, a/L)$ can be expanded perturbatively as a function of u in the weak coupling expansion,

$$\delta(u, a/L) = \delta_1(a/L)u + \delta_2(a/L)u^2 + \dots. \quad (2.2.7)$$

$\sigma(s, u)$ and $\Sigma(s, u, a/L)$ can also be expanded as functions of u in the form

$$\Sigma(s, u, a/L) = u + \Sigma^{(1)}(s, a/L)u^2 + \Sigma^{(2)}(s, a/L)u^3 + \dots, \quad (2.2.8a)$$

$$\sigma(s, u) = u + \sigma^{(1)}(s)u^2 + \sigma^{(2)}(s)u^3 + \dots. \quad (2.2.8b)$$

The one-loop coefficient $\Sigma^{(1)}(s, a/L)$ is defined as

$$\Sigma^{(1)}(s, a/L) \equiv p_1(sL/a) - p_1(L/a), \quad (2.2.9)$$

$$\sigma^{(1)}(s) = -2b_0, \quad (2.2.10)$$

where b_0 is the one-loop beta function, $b_0 = b_{0,0} + n_f b_{0,1}$. Here, $b_{0,0}$ is the gluonic contribution and $b_{0,1}$ is the fermionic contribution given by $b_{0,1} = \frac{2}{3} \frac{1}{(4\pi)^2}$. Substituting this relationship and Eq. (2.2.8) into Eq. (2.2.7), we obtain

$$\delta_1(a/L) = \Sigma^{(1)}(s, a/L) - \sigma^{(1)}(s), \quad (2.2.11)$$

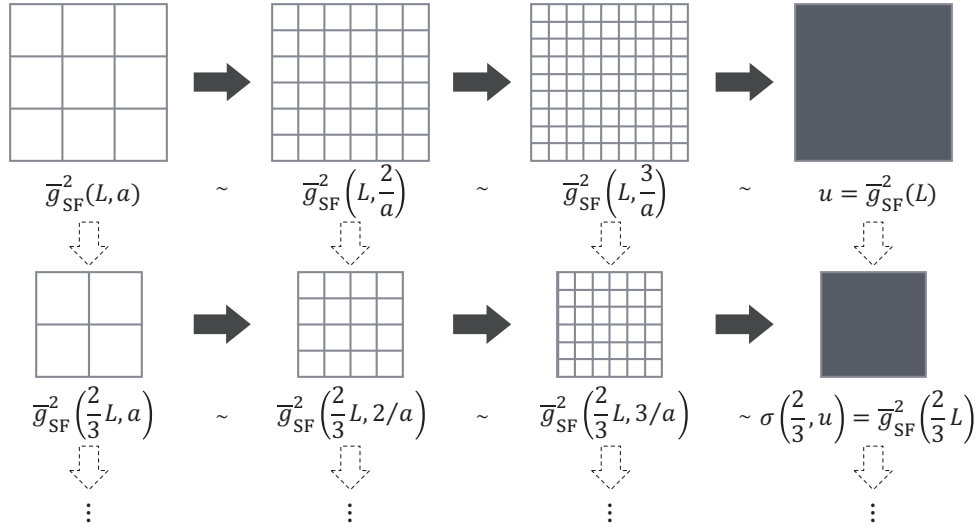


Figure 2.1: Schematic summarizing the process of obtaining take the continuum limit for the SSF using several lattices.

for the one-loop lattice artifact. $\delta_n(a/L)$ can be expressed as,

$$\delta_1(a/L) = \delta_{1,0}(a/L) + n_f \delta_{1,1}(a/L), \quad (2.2.12)$$

$$\delta_{1,1} = p_{1,1}(sL/a) - p_{1,1}(L/a) - 2b_{0,1} \ln s, \quad (2.2.13)$$

where $\delta_{1,0}(a/L)$ and $\delta_{1,1}(a/L)$ are the contributions from the pure gauge and fermion fields, respectively. At the continuum limit, $a \rightarrow 0$, $\delta_{1,1}(a/L)$ becomes zero, which leads to

$$\Sigma(s, a/L) \xrightarrow{a/L \rightarrow 0} b_{0,1} \ln s. \quad (2.2.14)$$

Figure 2.1 summarizes the process to take the continuum limit for the lattice step scaling function with a scaling factor of $s = 2/3$.

Chapter 3

The Möbius domain wall fermion

The lattice fermion satisfying the GW relation in Eq. (1.0.1) is termed the lattice chiral fermion, and the lattice chiral fermion operator was first proposed by Kaplan [17]. This operator is defined in five-dimensional space-time, with an extra dimension introduced in the spatial direction, and is referred to as the DWF operator. In continuum field theory, the action of the DWF is defined by

$$S_{\text{MB}} = \int d^4x \int_{-\infty}^{\infty} dx_5 \bar{\psi}(x, x_5) \left[\sum_{\mu=1}^5 \gamma_{\mu} \partial_{\mu} - m(x_5) \right] \psi(x, x_5), \quad (3.0.1)$$

where x_5 is the extra dimension coordinate and $m(x_5)$ is a mass depending on x_5 . Kaplan suggested that a positive mass, m_0 , in the positive region of the five-dimensional coordinate defined by $x_5 > 0$ and a negative mass, $-m_0$, in the negative region ($x_5 < 0$). The chiral fermion appears at the boundary between these two regions, $x_5 = 0$, as a four-dimensional operator. However, the boundary condition in the fifth-dimensional coordinate realized by the mass function $m(x_5)$ is not suited to lattice field theory. Thus, a new condition for the fifth direction was introduced by Furman and Shamir [18] and the formulation of the DWF in lattice field theory was completed. Furman and Shamir suggested a Dirichlet boundary condition for the fifth-dimensional finite space coordinates, defined from 0 to L_5 , and showed that the zero mode of the DWF appears on both boundaries of the fifth-dimensional coordinate.

The DWF includes many heavy modes and Furman and Shamir mentioned both the necessity and the manner of eliminating heavy modes from the DWF using the Pauli-Villars method, via lattice chiral symmetry and a chiral transformation. The effective four-dimensional operator, which is constructed so as to contain the lightest fermion mode with the Pauli-Villars method, satisfies the GW relation when the size of the fifth-dimensional lattice becomes infinity. Based on this approach, several different DWF operators have been proposed and simulations have been performed.

Brower et al. suggested the generalized form of the DWF, the Möbius domain wall fermion (MDWF), to introduce some parameters, and demonstrated that simulations using MDWFs are more computationally efficient than those employing certain DWFs [22, 23]. In the next

section, I summarize features of MDWFs with a periodic boundary condition so as to later compare MDWFs with the SF boundary condition. It should be noted that the lattice cutoff “ a ” is omitted in this section unless otherwise indicated.

3.1 Lattice Möbius domain wall fermion

The action of an MDWF is equivalent to the generalized action of a DWF. In lattice field theory, the action of an MDWF, \hat{S}_{MB} , is obtained using the lattice MDWF field $\hat{\psi}(n, n_s), \bar{\hat{\psi}}(n, n_s)$ [22, 23], written as

$$\begin{aligned} \hat{S}_{\text{MB}} &= \bar{\hat{\psi}}(n, n_s) D_{\text{MB}}(n, m; n_s, m_s) \hat{\psi}(m, m_s) \\ &= \sum_{n_s=1}^{N_5} \bar{\hat{\psi}}(n, n_s) D_{n_s}^+(n, m) \hat{\psi}(m, n_s) \\ &\quad + \sum_{n_s=2}^{N_5} \bar{\hat{\psi}}(n, n_s) D_{n_s}^-(n, m) P_R \hat{\psi}(m, n_s - 1) + \sum_{n_s=1}^{N_5-1} \bar{\hat{\psi}}(n, n_s) D_{n_s}^-(n, m) P_L \hat{\psi}(m, n_s + 1) \\ &\quad - m_f \bar{\hat{\psi}}(n, 1) D_{n_s}^-(n, m) P_R \hat{\psi}(m, N_5) - m_f \bar{\hat{\psi}}(n, n_s) D_{n_s}^-(n, m) P_L \hat{\psi}(m, 1), \end{aligned} \quad (3.1.1)$$

where n and m are the four-dimensional lattice coordinates, n_s and m_s are the fifth-dimensional lattice coordinates that run from 1 to N_5 , and m_f is the domain wall fermion mass. D_j^+ and D_j^- are the four-dimensional operators obtained from the Möbius parameters, b_j, c_j , as

$$D_j^+(n, m) = b_j D_{\text{WF}}(n, m) + \delta_{n,m}, \quad (3.1.2a)$$

$$D_j^-(n, m) = c_j D_{\text{WF}}(n, m) - \delta_{n,m}, \quad (j = 1, 2, \dots, N_5). \quad (3.1.2b)$$

Here, D_{WF} is the Wilson fermion operator defined in four dimension as

$$D_{\text{WF}}(n, m) = (-m_0 + 4)\delta_{n,m} - \frac{1}{2} \left[(1 - \gamma_\mu) U_\mu(n) \delta_{m, n+\mu} + (1 + \gamma_\mu) U_\mu^\dagger(m) \delta_{m, n-\mu} \right], \quad (3.1.3)$$

where m_0 is the domain wall negative mass (the domain wall height). In these calculations, we impose the periodic boundary condition for the Wilson fermion.

According to the zero mode solution of the MDWF, the left-handed zero mode is induced at $n_s = 1$ and the right-handed zero mode is induced at $n_s = N_5$. The quark field including the zero modes is defined from the MDWF field by

$$\hat{q}_n = P_L \hat{\psi}(n, 1) + P_R \hat{\psi}(n, N_5), \quad (3.1.4a)$$

$$\bar{\hat{q}}_n = \bar{\hat{\psi}}(n, 1) (-D_1^-) P_R + \bar{\hat{\psi}}(n, N_5) (-D_{N_5}^-) P_L. \quad (3.1.4b)$$

The mass of the MDWF can be introduced as $m_f \bar{\hat{q}}_n \hat{q}_n$. The five-dimensional structure of the action can be reinterpreted as a many-flavor fermion system in which flavors interact with one

an other, by translating the five-dimensional index, s . From the mass matrix of the many-flavor system, we find that the lightest mass mode of the four-dimensional fermion is localized at $n_s = 1$ and N_5 when $m_f = 0$. In addition, the left-handed mode is localized at $n_s = 1$ and the right-handed mode at $n_s = N_5$. By combining the left- and right-handed modes localized at both boundaries as Eq. (3.1.4), we can construct an effective four-dimensional fermion field $\hat{q}, \tilde{\hat{q}}$. Thus, the terms proportional to m_f in Eq. (3.1.1) provide a mixture of the left- and right-handed modes of the four-dimensional fermion, namely the Dirac mass term.

When $N_5 = 6$, the matrix form in the fifth-dimensional direction is given by

$$D_{\text{MB}}(n, m) = \begin{pmatrix} D_1^+ & D_1^- P_L & 0 & 0 & 0 & -m_f D_1^- P_R \\ D_2^- P_R & D_2^+ & D_2^- P_L & 0 & 0 & 0 \\ 0 & D_3^- P_R & D_3^+ & D_3^- P_L & 0 & 0 \\ 0 & 0 & D_4^- P_R & D_4^+ & D_4^- P_L & 0 \\ 0 & 0 & 0 & D_5^- P_R & D_5^+ & D_5^- P_L \\ -m_f D_6^- P_L & 0 & 0 & 0 & D_6^- P_R & D_6^+ \end{pmatrix} (n, m). \quad (3.1.5)$$

The chiral transformation in the four-dimensional theory is given by

$$\hat{q}_n \rightarrow e^{i\theta\gamma_5} \hat{q}_n, \quad \tilde{\hat{q}}_n \rightarrow \tilde{\hat{q}}_n e^{i\theta\gamma_5}. \quad (3.1.6)$$

In order to reinterpret this chiral transformation for the four-dimensional field in terms of the five-dimensional domain wall fermion field, Eq. (3.1.6) is substituted into Eq. (3.1.4), to give

$$\hat{q}'_n = (1 + i\theta\gamma_5)q_n = (1 - i\theta)P_L\hat{\psi}(n, 1) + (1 + i\theta)P_R\hat{\psi}(n, N_5), \quad (3.1.7a)$$

$$\tilde{\hat{q}}'_n = \tilde{\hat{q}}_n(1 + i\theta\gamma_5) = \bar{\psi}(n, 1)(-D_1^-)P_R(1 + i\theta) + \bar{\hat{q}}(n, N_5)(-D_{N_5}^-)P_L(1 - i\theta), \quad (3.1.7b)$$

where $\theta \ll 1$ is assumed. Hence, the chiral transform of boundary fields, $\hat{\psi}(n, 1)$ and $\hat{\psi}(n, N_5)$, can be defined and the chiral transform of the MDWF field is defined by

$$\hat{\psi}'(n, n_s) = (\mathbf{1} + i\theta\Gamma)_{n_s, m_s} \hat{\psi}(n, m_s), \quad (3.1.8a)$$

$$\tilde{\hat{\psi}}'(n, n_s) = \tilde{\hat{\psi}}(n, m_s)(\mathbf{1} - i\theta\Gamma)_{m_s, n_s}, \quad (3.1.8b)$$

where Γ is the chiral transition operator for the fifth-dimensional direction and defined by

$$\Gamma = \begin{pmatrix} -1 & 0 & 0 & 0 & 0 & 0 \\ 0 & -1 & 0 & 0 & 0 & 0 \\ 0 & 0 & -1 & 0 & 0 & 0 \\ 0 & 0 & 0 & 1 & 0 & 0 \\ 0 & 0 & 0 & 0 & 1 & 0 \\ 0 & 0 & 0 & 0 & 0 & 1 \end{pmatrix}, \quad (3.1.9)$$

in the case of $N_5 = 6$. When $m_f = 0$, the chiral transformation of the MDWF action for the operator Eq. (3.1.5) is given by the operator Γ , written as

$$[D_{\text{MB}}, \Gamma] = \left(2D_{N_5/2}^- P_L \delta_{n_s, N_5/2} \delta_{m_s, N_5/2+1} - 2D_{N_5/2+1}^- P_R \delta_{n_s, N_5/2+1} \delta_{m_s, N_5/2} \right). \quad (3.1.10)$$

The terms on the right hand side of Eq. (3.1.10) represent the contribution of the heavy fermion mode and disappear when N_5 is infinite. As a result, the MDWF is invariant with regard to the chiral transformation in five-dimensional space at the limit of $N_5 \rightarrow \infty$.

The MDWF operator should satisfy discrete space-time symmetries; the charge conjugation C , parity symmetry P , time reversal T and Γ_5 -Hermiticity. Γ_5 -Hermiticity is an extension of γ_5 -Hermiticity in the four-dimensional Euclidean field theory to the MDWF, written as

$$\Gamma_5 = \gamma_5 \mathcal{R} D^-, \quad D^- = \text{diag}[D_1^-, D_2^-, \dots, D_{N_5}^-]. \quad (3.1.11)$$

Hence, the symmetry of the Γ_5 Hermite transformation is defined by

$$\Gamma_5 D_{\text{MB}} \Gamma_5 = D_{\text{MB}}^\dagger. \quad (3.1.12)$$

3.2 The effective four-dimensional operator

The MDWF has N_5 fermion modes but only the lightest mode is equivalent to the chiral fermion. Furman and Shamir suggested that the Pauli-Villars method can be used to remove heavy modes from the MDWF operator, as

$$D_{\text{PV}}^{-1} D_{\text{MB}}, \quad (3.2.1)$$

where D_{PV} is the MDWF operator, with $m_f = 1$ [18]. The partition function has the same form for the MDWF operator and the operator in Eq. (3.2.1). Moreover the operator in Eq. (3.2.1) satisfies the GW relation [58, 59]. Boriçi proposed the effective four-dimensional operator

$$D_{\text{eff}} = \epsilon^T P^T D_{\text{PV}}^{-1} D_{\text{MB}} P \epsilon, \quad (3.2.2)$$

where P is a permutation and chiral projection operator and ϵ is a projection operator from the five-dimensional matrix to the four-dimensional one, written as

$$P = \begin{pmatrix} P_L & P_R & 0 & 0 & 0 & 0 \\ 0 & P_L & P_R & 0 & 0 & 0 \\ 0 & 0 & P_L & P_R & 0 & 0 \\ 0 & 0 & 0 & P_L & P_R & 0 \\ 0 & 0 & 0 & 0 & P_L & P_R \\ P_R & 0 & 0 & 0 & 0 & P_L \end{pmatrix}, \quad \epsilon = \begin{pmatrix} 1 \\ 0 \\ 0 \\ 0 \\ 0 \\ 0 \end{pmatrix}. \quad (3.2.3)$$

The effective four-dimensional operator is equivalent to the lattice chiral fermion operator having the lightest fermion mode extracted by the Pauli-Villars method. The form $P^T D_{\text{PV}}^{-1} D_{\text{MB}} P$ looks like a tridiagonal matrix in the fifth-dimensional matrix representation.

After some algebra D_{eff} can be written as in the following form.

$$D_{\text{eff}} = \frac{1 + m_f}{2} - \frac{1 - m_f}{2} \gamma_5 U(\mathcal{H}_{\omega(j)}), \quad (3.2.4)$$

$$U(x) = \frac{\prod_{j=1}^{N_5} (1 + x) + \prod_{j=1}^{N_5} (1 - x)}{\prod_{j=1}^{N_5} (1 + x) - \prod_{j=1}^{N_5} (1 - x)}, \quad (3.2.5)$$

$$\mathcal{H}_{\omega(j)} \equiv \gamma_5 \frac{(b_j + c_j) D_{\text{WF}}}{(b_j - c_j) D_{\text{WF}} + 2}, \quad (3.2.6)$$

where $\mathcal{H}_{\omega(j)}$ is a kernel operator constructed from lattice fermion operators. In the case that N_5 is infinity, $U(x)$ becomes the sign function and the effective four-dimensional operator agrees with the overlap fermion operator, meaning

$$D_{\text{OV}} = \frac{1 + m_f}{2} - \frac{1 - m_f}{2} \gamma_5 \text{sgn}(\mathcal{H}_{\omega}). \quad (3.2.7)$$

The massless overlap fermion operator satisfies the GW relation in Eq. (1.0.1) completely such that

$$\begin{aligned} D_{\text{OV}} \gamma_5 + \gamma_5 D_{\text{OV}} &= \frac{1}{2} (1 - \gamma_5 \text{sgn}(\mathcal{H}_{\omega})) \gamma_5 + \gamma_5 \frac{1}{2} (1 - \gamma_5 \text{sgn}(\mathcal{H}_{\omega})) \\ &= \gamma_5 - \frac{1}{2} (\gamma_5 \text{sgn}(\mathcal{H}_{\omega}) \gamma_5 + \text{sgn}(\mathcal{H}_{\omega})), \end{aligned} \quad (3.2.8)$$

$$\begin{aligned} 2D_{\text{OV}} \gamma_5 D_{\text{OV}} &= \frac{1}{2} (1 - \gamma_5 \text{sgn}(\mathcal{H}_{\omega})) \gamma_5 (1 - \gamma_5 \text{sgn}(\mathcal{H}_{\omega})) \\ &= \gamma_5 - \frac{1}{2} (\gamma_5 \text{sgn}(\mathcal{H}_{\omega}) \gamma_5 + \text{sgn}(\mathcal{H}_{\omega})). \end{aligned} \quad (3.2.9)$$

The kernel operator, \mathcal{H}_{ω} , has several specific patterns, as follows.

1. The Shamir DWF

This corresponds to the DWF firstly defined by Shamir and Furman [18]. In many papers, it is described simply as *the domain wall fermion (DWF)*. In this case, the Möbius parameters are set to $b_j = a_5$ and $c_j = 0$, where a_5 is a coefficient typically given a value of 1. The kernel operator is given by

$$\mathcal{H}_{\omega(j)} = \gamma_5 \frac{D_{\text{WF}}}{D_{\text{WF}} + 2}. \quad (3.2.10a)$$

2. The Boriçi DWF

Boriçi proposed this formulation, in which the kernel operator is different from that for the Shamir DWF [60, 61, 62]. Here, the Möbius parameters are set to $b_j = c_j = a_5$ and kernel operator is given by

$$\mathcal{H}_{\omega(j)} = \gamma_5 D_{\text{WF}}. \quad (3.2.10b)$$

3. The optimal Shamir DWF

The Möbius parameters for this DWF, b_j and c_j , are determined so as to approximate the sign functions by setting $b_j + c_j = \omega_j$ and $b_j - c_j = a_5$, where ω_j is a coefficient depending on the fifth-dimensional lattice index [63]. This optimized DWF can more fully satisfy lattice chiral symmetry in finite lattice space compared to the Shamir DWF based on the selection of appropriate values of b_j and c_j . The kernel operator is similar to that for the Shamir DWF, and is given by

$$\mathcal{H}_{\omega(j)} = \gamma_5 \frac{\omega_j D_{\text{WF}}}{a_5 D_{\text{WF}} + 2}. \quad (3.2.10c)$$

4. The optimal Boriçi DWF

Similar to the optimal Shamir DWF, the Möbius parameters are determined by sign approximation functions with $b_j = c_j = \omega_j$ [63]. The kernel operator is also similar to that for the Boriçi DWF, written as

$$\mathcal{H}_{\omega(j)} = \gamma_5 \omega_j D_{\text{WF}}. \quad (3.2.10d)$$

Values of ω_j are selected so as to approximate a sign function with $U(x)$ in Eq. (3.2.5) at a small N_5 value. There are several approximation methods for the sign function. In this the present work, the Zolotarev approximation was employed for sign function approximation. However, this method cannot be used in conjunction with the SF scheme for MDWFs, as discussed in Chapter 5.

Now I note the effective four-dimensional operator at the continuum limit [64]. The lattice cutoff, a , is specified in the term in Eq. (3.2.4) as,

$$aD_{\text{eff}} = \frac{1 + am_f}{2} - \frac{1 - am_f}{2} \gamma_5 U(a\mathcal{H}_{\omega(j)}). \quad (3.2.11)$$

In the case that a is small, D_{eff} in Eq. (3.2.11) can be expanded with a . The expanded form up to $O(a^2)$ at the tree-level is represented as

$$aD_{\text{eff}} \rightarrow Z [ia\cancel{\partial} + am_{\text{res}}], \quad (3.2.12)$$

where Z is a renormalization factor and m_{res} is a residual mass and they become,

$$Z = \frac{(1 - am_f)U(x_{m_0})}{(am_0)(2 - (am_0)a_5)}, \quad (3.2.13)$$

$$am_{\text{res}} = \left[\frac{1 + am_f}{1 - am_f} \frac{1}{U(x_{m_0})} - 1 \right] \frac{(am_0)(2 - (am_0)a_5)}{2}, \quad (3.2.14)$$

$$x_{m_0} = \frac{(am_0)}{2 - (am_0)a_5}. \quad (3.2.15)$$

m_{res} varies with the degree of freedom of the fifth-dimensional lattice indices and approaches zero as N_5 becomes larger. When m_{res} has a finite value, the DWF cannot recover the

continuum massless Dirac operator at the continuum limit. Hence, we must set m_f to satisfy the relationship, $m_{res} = 0$. For the Shamir DWF with $am_0 = 1.0$ and $a_5 = 1$, in particular, m_{res} does not depend on the number of fifth-dimensional lattice points, and becomes $m_{res} = 0$ when $m_f = 0$ incidentally. To construct the SF scheme using an MDWF with a finite size of N_5 , renormalization at the tree-level is required, and this is discussed in Section 6.2.

Chapter 4

Lattice chiral symmetry in the SF scheme

4.1 The universality argument

In this section, I introduce requirements for the lattice fermion in the SF scheme based on the universality argument [39]. For the SF scheme, the SF boundary condition in Eqs. (2.1.5) does not satisfy chiral symmetry. Thus, the chiral symmetry should be broken explicitly at the temporal boundaries in the SF scheme. On the lattice, the lattice chiral symmetry should be also broken explicitly at the temporal boundaries. Therefore, the GW relation (which is a realization of lattice chiral symmetry) must be modified at the temporal boundaries in the SF scheme, as

$$\gamma_5 D + D \gamma_5 = a D \gamma_5 D + \gamma_5 P_{\text{SF}}, \quad (4.1.1)$$

$$P_{\text{SF}} \psi(x) \equiv \frac{1}{a} (\delta_{x_4, a} P_- \psi(\mathbf{x}, x_4 = a) + \delta_{x_4, T-a} P_+ \psi(\mathbf{x}, x_4 = T - a)). \quad (4.1.2)$$

The operator P affects only the temporal boundaries, $x_0 = 0$ and T , at the continuum limit. This means that the chiral symmetry of the operator satisfying Eq. (4.1.1) is broken at the time boundary only, whereas, in time bulk regions, symmetry is maintained due to the original GW relation. Multiplying the quark propagators on both sides of Eq. (4.1.1) takes the continuum limit as $a \rightarrow 0$, the modified GW relation for the lattice Dirac operator leads to

$$\gamma_5 S(x, y) + S(x, y) \gamma_5 = \int_{z_4=0} dz S(x, z) \gamma_5 P_- S(z, y) + \int_{z_4=T} dz S(x, z) \gamma_5 P_+ S(z, y). \quad (4.1.3)$$

Several formulations of the boundary operator P_{SF} are discussed by Taniguchi [37, 38] using an orbifolding method, and by Lüscher [39] with an universality argument. One condition for lattice fermion actions in the SF scheme is that the lattice Dirac propagator should satisfy Eq. (4.1.3) at the continuum limit. Several modifications to the lattice chiral fermion actions that reproduce the SF boundary condition are discussed in Refs. [38, 37, 39, 41].

4.2 $O(a)$ improvement

On-shell improved theory is a well-known method that adds $O(a)$ counter terms to cancel the $O(a)$ cutoff effect of the on-shell quantities [65]. The coefficient of each counter term is determined by the PCAC relation in continuum theory, as

$$\partial_\mu A_\mu^a = 2mP^a, \quad (4.2.1)$$

where $A_\mu^a(x)$ is the axial vector current and $P^a(x)$ is the pseudo scalar density with the adjoining representation a in the flavor $SU(3)$ symmetry. Using the $SU(3)$ group generator, T^a , these are defined by

$$A_\mu^a(x) = \bar{\psi}(x)\gamma_\mu\gamma_5 T^a\psi(x), \quad (4.2.2)$$

$$P^a(x) = \bar{\psi}(x)\gamma_5 T^a\psi(x). \quad (4.2.3)$$

As the $O(a)$ counter terms depend on the quark mass, a mass-independent scheme is desirable when implementing the $O(a)$ improvement based on the PCAC relation. However, the naive procedure of the mass-independent scheme cannot optimize the $O(a)$ error completely. This problem is solved by modifying the bare coupling, g_0 , and the bare quark mass, m_q [66], as

$$\tilde{g}_0^2 = g_0^2(1 + b_g am_q), \quad (4.2.4)$$

$$\tilde{m}_q = m_q(1 + b_m am_q). \quad (4.2.5)$$

Here, b_g and b_m are coefficients tuned so as to eliminate the cutoff effect at $O(a)$. In the improved mass-independent renormalization method, the renormalized coupling and quark mass are defined by

$$g_R^2 = \tilde{g}_0^2 Z_g(\tilde{g}_0^2, a\mu), \quad (4.2.6)$$

$$m_R = \tilde{m}_q Z_m(\tilde{g}_0^2, a\mu), \quad (4.2.7)$$

where Z_g and Z_m are the renormalization constants. In the SF scheme, the temporal boundary field $\xi(\mathbf{x})$ is also renormalized along with $A_\mu^a(x)$ and $P^a(x)$. Using the improved bare coupling \tilde{g}_0^2 , the renormalization expressions for $A_\mu^a(x)$, $P^a(x)$ and $\xi(\mathbf{x})$ are

$$\xi_R(\mathbf{x}) = Z_\xi(\tilde{g}_0^2, a\mu)(1 + b_\xi am_q)\xi(\mathbf{x}), \quad (4.2.8)$$

$$(A_R)_\mu^a(x) = Z_A(\tilde{g}_0^2, a\mu)(1 + b_A am_q)\{A(x)_\mu^a + \delta A_\mu^a\}, \quad (4.2.9)$$

$$(P_R)^a(x) = Z_P(\tilde{g}_0^2, a\mu)(1 + b_P am_q)P^a. \quad (4.2.10)$$

Here, $Z_C(\tilde{g}_0^2, a\mu)$ is a renormalization constant and b_C is a coefficient ($C = \xi, A, \text{ or } P$). From the PCAC relation Eq (4.2.1), it is expected that the correlation functions $(A_R)_\mu^a(x)$ and $(P_R)^a(x)$ have the relation,

$$\left\langle \frac{1}{2}(\partial_\mu^* + \partial_\mu)(A_R)_\mu^a(x)\mathcal{O} \right\rangle = 2m_R \langle (P_R)^a(x)\mathcal{O} \rangle + O(a^2), \quad (4.2.11)$$

where \mathcal{O} is an interpolating operator that does not overlap the coordinate x . If the coefficients of the $O(a)$ counter terms are tuned, the renormalized quark mass has a cutoff effect at $O(a^2)$ and is described by

$$m_R = m \frac{Z_A(1 + b_A a m_q)}{Z_P(1 + b_P a m_q)} + O(a^2), \quad (4.2.12)$$

$$m = \frac{1}{2} \frac{\frac{1}{2}(\partial_0^* + \partial_0)f_A(x_0) + c_{AA}a\partial_0^*\partial_0 f_P(x_0)}{f_P(x_0)}. \quad (4.2.13)$$

In perturbation theory, the renormalized correlation functions, $[f_A(x_0)]_R, [f_P(x_0)]_R$, are expanded by g_R^2 , as

$$[f_A(x_0)]_R = f_A^{(0)}(x_0) + g_R^2 \left\{ f_A^{(1)}(x_0) + m_c^{(1)} \frac{\partial}{\partial m_0} f_A^{(0)} + (Z_A^{(1)} + 2Z_\xi^{(1)})f_A^{(0)}(x_0) + a f_{\delta A}^{(1)}(x_0) \right\} + O(g_R^4), \quad (4.2.14)$$

$$[f_P(x_0)]_R = f_P^{(0)}(x_0) + g_R^2 \left\{ f_P^{(1)}(x_0) + m_c^{(1)} \frac{\partial}{\partial m_0} f_P^{(0)} + (Z_P^{(1)} + 2Z_\xi^{(1)})f_P^{(0)}(x_0) \right\} + O(g_R^4), \quad (4.2.15)$$

$$f_A^{(0)}(x_0) = a^6 \sum_{a=1}^{N_f} \sum_{\mathbf{y}, \mathbf{z}} \frac{1}{N_f^2 - 1} \left\langle A_0^a(x) \bar{\xi}(\mathbf{y}) \gamma_5 \frac{1}{2} \tau^a \xi(\mathbf{z}) \right\rangle, \quad (4.2.16)$$

$$f_P^{(0)}(x_0) = a^6 \sum_{a=1}^{N_f} \sum_{\mathbf{y}, \mathbf{z}} \frac{1}{N_f^2 - 1} \left\langle P^a(x) \bar{\xi}(\mathbf{y}) \gamma_5 \frac{1}{2} \tau^a \xi(\mathbf{z}) \right\rangle. \quad (4.2.17)$$

Here the details of the one-loop corrections, $f_A^{(1)}(x_0)$ and $f_P^{(1)}(x_0)$ are omitted. From the above, $[f_A(x_0)]_R$ and $[f_P(x_0)]_R$ are $O(a)$ have improvements in $O(a)$ provided that the proper values are selected for the coefficients for the $O(a)$ counter terms.

In the case of a free quark in continuum theory without a classical background field, we can obtain $f_A^{(0)}$ and $f_P^{(0)}$ analytically because the propagator, $S(x, y)$, can be solved analytically, according to

$$f_A^{(0)}(x_4) = -\frac{N}{R^2} [E^2 - m^2 + m\{m \cosh(2E(T - x_4)) + E \sinh(2E(T - x_4))\}], \quad (4.2.18)$$

$$f_P^{(0)}(x_4) = \frac{NE}{R^2} [E \cosh(2E(T - x_4)) + m \sinh(2E(T - x_4))], \quad (4.2.19)$$

$$R = E \cosh(ET) + m \sinh(ET), \quad E = \sqrt{\mathbf{p}_0^2 + m^2}, \quad \mathbf{p}_0 = \left(\frac{\theta_1}{L}, \frac{\theta_2}{L}, \frac{\theta_3}{L} \right). \quad (4.2.20)$$

When we set $T = 2L, m = 0$, and $\theta_1 = \theta_2 = \theta_3 = \theta$, the ratio of $f_A(T/2)$ to $f_P(T/2)$ depends solely on the spatial phase, meaning

$$\frac{f_A(\frac{T}{2})}{f_P(\frac{T}{2})} = -\frac{1}{\cosh(2\sqrt{3}\theta)}. \quad (4.2.21)$$

Chapter 5

Set up of the SF scheme with the MDWFs

5.1 Construction of the operator

In this section, I introduce the construction of the SF scheme for the MDWFs based on the universality argument in the SF scheme introduced for the lattice chiral fermion in Section. 4.1. Takeda constructed the SF boundary operator, B_{DWF} , by extending the boundary operator P for the four-dimensional overlap operator defined in Eq. (4.1.2) to the five-dimensional form for the DWF as follows [41], as

$$B_{\text{DWF}}(n, m; n_s, m_s) = B(n, m)(\Gamma\mathcal{R})(n_s, m_s), \quad (5.1.1)$$

$$B(n, m) = \delta_{n,m} \gamma_5 (\delta_{n_4,1} P_- + \delta_{n_4, N_T-1} P_+). \quad (5.1.2)$$

In the case of $N_5 = 6$, the five-dimensional matrix form of $\Gamma\mathcal{R}$ is given by

$$\Gamma\mathcal{R} = \begin{pmatrix} 0 & 0 & 0 & 0 & 0 & -1 \\ 0 & 0 & 0 & 0 & -1 & 0 \\ 0 & 0 & 0 & -1 & 0 & 0 \\ 0 & 0 & 1 & 0 & 0 & 0 \\ 0 & 1 & 0 & 0 & 0 & 0 \\ 1 & 0 & 0 & 0 & 0 & 0 \end{pmatrix}. \quad (5.1.3)$$

Takeda constructed the DWF operator with the SF boundary term, written as

$$D_{\text{DWF}}^{\text{SF}}(n, m; n_s, m_s) = D_{\text{DWF}}(n, m; n_s, m_s) + c_{\text{SF}} B_{\text{DWF}}(n, m; n_s, m_s), \quad (5.1.4)$$

where c_{SF} is a coefficient of the SF boundary term tuned based on the PCAC relation [42, 43, 44, 45]. The block anti-diagonal form and the sign in the five-dimensional block form of the matrix in Eq. (5.1.1) are determined so as to break the lattice chiral symmetry of the DWF and to maintain the universality argument that keeps the lattice discrete symmetries (C, P, T and Γ_5 -Hermiticity) in the SF scheme. The lattice chiral symmetry of $B_{\text{DWF}}(n, m; n_s, m_s)$

should be noted. In the case of the chiral transformation of the operator in Eq. (3.1.9), the chiral transformation of the SF boundary operator B_{DWF} is

$$[B_{\text{DWF}}, \Gamma] = (-2B\delta_{n_s, N_5+1-m_s}), \quad (5.1.5)$$

and does not vanish even though N_5 is infinite. From Eq. (3.1.10), the DWF operator (the MDWF with $(b_j, c_j) = (1, 0)$) satisfies lattice chiral symmetry as $N_5 \rightarrow \infty$. However, the DWF with the SF boundary term B_{DWF} cannot satisfy lattice chiral symmetry because of B .

I further extend the boundary operator B_{DWF} defined for the standard domain wall fermion to the MDWF of Eq. (3.1.5) and propose the MDWF in the SF scheme. For D_{MB} , the ordering of the coefficients of b_j and c_j or $D_j^{+/-}$ in the fifth dimension is arbitrary in the periodic or infinite space-time volume, and this ordering does not affect the form of the effective four-dimensional operator as seen in Eqs. (3.1.5) and (3.2.2). However, in the SF scheme, parity symmetry in the fifth direction is required for the ordering so as to satisfy the universality argument. I therefore employed an MDWF having the fifth-dimensional parity symmetry, \mathring{D}_{MB} , for the SF scheme, written as

$$\mathring{D}_{\text{MB}}(n, m) = \begin{pmatrix} D_1^+ & D_1^- P_L & 0 & 0 & 0 & -m_f D_1^- P_R \\ D_2^- P_R & D_2^+ & D_2^- P_L & 0 & 0 & 0 \\ 0 & D_3^- P_R & D_3^+ & D_3^- P_L & 0 & 0 \\ 0 & 0 & D_3^- P_R & D_3^+ & D_3^- P_L & 0 \\ 0 & 0 & 0 & D_2^- P_R & D_2^+ & D_2^- P_L \\ -m_f D_1^- P_L & 0 & 0 & 0 & D_1^- P_R & D_1^+ \end{pmatrix} (n, m). \quad (5.1.6)$$

The Zolotarev approximation function used for the operator, \mathring{D}_{MB} , must be modified under the SF boundary condition and this issue is discussed in Secion. 5.2. I propose that the MDWF operator in the SF scheme can be defined by

$$D_{\text{MB}}^{\text{SF}}(n, m; n_s, m_s) = \mathring{D}_{\text{MB}}(n, m; n_s, m_s) + c_{\text{SF}} B_{\text{SF}}(n, m; n_s, m_s), \quad (5.1.7)$$

and

$$B_{\text{SF}} = \begin{pmatrix} 0 & 0 & 0 & 0 & 0 & -D_1^{(-)} B \\ 0 & 0 & 0 & 0 & -D_2^{(-)} B & 0 \\ 0 & 0 & 0 & -D_3^{(-)} B & 0 & 0 \\ 0 & 0 & D_3^{(-)} B & 0 & 0 & 0 \\ 0 & D_2^{(-)} B & 0 & 0 & 0 & 0 \\ D_1^{(-)} B & 0 & 0 & 0 & 0 & 0 \end{pmatrix}. \quad (5.1.8)$$

The Wilson fermion contained in \mathring{D}_{MB} in Eq. (5.1.6) is defined for the time dimension in $n_4 = 1, 2, \dots, N_T - 1$. The universality argument does not completely determine the form of the boundary term B_{SF} , because the ordering of the coefficients c_j and b_j or $D_j^{+/-}$ is still arbitrary as far as parity symmetry in the fifth dimension is imposed. I also construct

another boundary operator, B_{SF} , such that the four-dimensional boundary operator, $B(n, m)$, is present only on both edges in the fifth direction [55];

$$B_{\text{SF}}(n, m) = \begin{pmatrix} 0 & 0 & 0 & 0 & 0 & -D_1^{(-)}B \\ 0 & 0 & 0 & 0 & 0 & 0 \\ 0 & 0 & 0 & 0 & 0 & 0 \\ 0 & 0 & 0 & 0 & 0 & 0 \\ 0 & 0 & 0 & 0 & 0 & 0 \\ D_1^{(-)}B & 0 & 0 & 0 & 0 & 0 \end{pmatrix} (n, m). \quad (5.1.9)$$

With the periodic boundary condition in all space-time dimensions, we can obtain the four-dimensional effective overlap operator in Eq. (3.2.4) analytically from the MDWF. It is helpful to clarify the violation of the GW relation in the time direction with regard to the four-dimensional operator of the MDWF. However, it appears to be impossible to extract the four-dimensional effective form as a compact and analytic operator from for the MDWF operator in the SF scheme, because the boundary operator, B_{SF} , in Eq. (5.1.8) has an anti-diagonal form which prevents this extraction from occurring analytically. Here, I define an effective four-dimensional operator by using the renormalization factor in Eqs. (3.2.13) and (3.2.14), written as

$$aD_q \equiv Z^{-1} aD_{\text{eff}}(am_{\text{cr}}), \quad (5.1.10)$$

where m_{cr} is a specific value of m_f set so that $m_{\text{res}} = 0$.

5.2 Rearrangements of the Zolotarev sign function approximation

In the SF scheme, the MDWF is imposed parity symmetry in the fifth dimension, meaning that we cannot use the Zolotarev sign function approximation method to determine the coefficient ω_j in Eqs. (3.2.10c) and (3.2.10d). Zolotarev's method is the most accurate sign function approximation. Because of what the MDWF using the coefficients b_j and c_j allows lattice chiral symmetry with minimal computational cost. Here, I introduce a modification of Zolotarev's method that satisfies the requirement for parity symmetry and investigate the accuracy of this modified approach. The original Zolotarev approximation method is described in Appendix B.

In the case of the optimal DWF type of MDWF, the coefficients b_j and c_j are obtained from ω_j as tuned using Zolotarev's method. In order to determine w_j with the Zolotarev approximation, we need the approximation range of the sign function. The range of the matrix sign function, $\text{sgn}(\mathcal{H}_\omega)$, is determined by the highest and lowest eigenvalues of \mathcal{H}_ω and the sign approximation function, $R_{N_5}(\mathcal{H}_\omega)$, is given by

$$R_{N_5}(\mathcal{H}_\omega) = \frac{\prod_{j=1}^{N_5} (1 + \omega_j \mathcal{H}_\omega) - \prod_{j=1}^{N_5} (1 - \omega_j \mathcal{H}_\omega)}{\prod_{j=1}^{N_5} (1 + \omega_j \mathcal{H}_\omega) + \prod_{j=1}^{N_5} (1 - \omega_j \mathcal{H}_\omega)}. \quad (5.2.1)$$

To evaluate the accuracy of the approximation, I introduce the metric

$$\delta_Z^{N_5}(x) \equiv |\text{sgn}(x) - R_{N_5}(x)|. \quad (5.2.2)$$

Due to the parity symmetry in the fifth dimension, the set up of the MDWF with N_5 in the SF scheme requires that ω_j is determined so as to satisfy the relation,

$$\omega_j = \omega_{N_5-j+1} \quad (j = 1, 2, \dots, N_5/2). \quad (5.2.3)$$

The sign approximation function in Eq. (5.2.1) is modified to

$$\tilde{R}_{N_5}(x) = \frac{\prod_{j=1}^{N_5/2} (1 + \omega_j \mathcal{H}_\omega)^2 - \prod_{j=1}^{N_5/2} (1 - \omega_j \mathcal{H}_\omega)^2}{\prod_{j=1}^{N_5/2} (1 + \omega_j \mathcal{H}_\omega)^2 + \prod_{j=1}^{N_5/2} (1 - \omega_j \mathcal{H}_\omega)^2}. \quad (5.2.4)$$

I refer to this form as quasi-optimal sign approximation function ¹.

The accuracy of the sign approximation function is related to the accuracy of the chiral symmetry of the MDWF. Here, I discuss the relationship between the accuracy of the sign approximation and the quasi-optimal sign approximation functions. From Eqs. (5.2.1) and (5.2.4), it is evident that the quasi-optimal sign approximation function can be expressed using the Zolotarev sign approximation as

$$\tilde{R}_{N_5}(x) = \frac{2R_{N_5/2}(x)}{(R_{N_5/2}(x))^2 + 1}. \quad (5.2.5)$$

I define $\delta_{\text{QZ}}^{N_5}$ as the error associated with the quasi-optimal sign approximation function, written as

$$\delta_{\text{QZ}}^{N_5}(x) \equiv \text{sgn}(x) - \tilde{R}_{N_5}(x). \quad (5.2.6)$$

The magnitude of $\delta_{\text{QZ}}^{N_5}(x)$ is analytically estimated using Eqs. (5.2.4) and (5.2.2) as,

$$|\delta_{\text{QZ}}^{N_5}(x)| \leq \frac{(\delta_{N_5/2})^2}{2(1 - \delta_{N_5/2}) + (\delta_{N_5/2})^2}. \quad (5.2.7)$$

These calculations demonstrate that the accuracy of the quasi-optimal sign approximation function is on the same order as that of the Zolotarev sign approximation function.

5.3 The expression of the fermionic contribution $p_{1,1}$

The fermionic contribution of the renormalized SF coupling constant, $p_{1,1}$, is calculated using the operator constructed in Eq. (5.1.7) to check the universality argument. With the MDWF

¹The MDWF is obtained using a quasi-optimal sign approximation in conjunction with a dynamical simulation [67, 68]

operator in the five-dimensional lattice, the fermionic contribution, $p_{1,1}$, is defined by

$$\begin{aligned} p_{1,1} &= \frac{1}{k} \frac{\partial}{\partial \eta} \left[\text{Tr} \ln \left[Z^{-1} D_{\text{PV}}^{-1} D_{\text{MB}}^{\text{SF}} \right] \right] \\ &= \frac{1}{k} \sum_{\mathbf{p}} \text{Tr} \left[\frac{\partial \tilde{D}_{\text{MB}}^{\text{SF}}}{\partial \eta} (\tilde{D}_{\text{MB}}^{\text{SF}})^{-1} - \frac{\partial \tilde{D}_{\text{PV}}}{\partial \eta} (\tilde{D}_{\text{PV}})^{-1} \right], \end{aligned} \quad (5.3.1)$$

where \tilde{D} indicates the MDWF operator with the momentum representation for the spatial direction and the trace affects on the five-dimensional lattice, spinor and color indices. In this section, I omit the substitution of $\eta = 0$ after the differentiation by η for the sake of simplicity, just as in Eq. (5.3.1). The effective four-dimensional operator is obtained from the MDWF operator, then Eq. (5.3.1) must agree with that one calculated from the effective four-dimensional operator. In this section, I demonstrate the equivalence of $p_{1,1}$ constructed with the MDWF operator and that with the effective four-dimensional operator.

I give the one-loop contribution to the effective action induced from the action with the effective four-dimensional operator $p_{1,1}^{\text{eff}}$ to distinguish it from Eq. (5.3.1), and is written as

$$p_{1,1}^{\text{eff}} = \frac{1}{k} \frac{\partial}{\partial \eta} \left[\text{tr} \ln \left[\tilde{D}_q \right] \right], \quad (5.3.2)$$

where \tilde{D}_q is the momentum representation for the spatial direction D_q defined in Eq. (5.1.10) and the trace is taken on the four-dimensional lattice sites, color, and spinor indices. The effective four-dimensional operator is renormalized by Z and am_{res} according to Eqs. (3.2.13)-(3.2.15). Below, I demonstrate that $p_{1,1} = p_{1,1}^{\text{eff}}$.

Substituting Eqs. (3.2.2) and (5.1.10) into Eq. (5.3.2), we have

$$\begin{aligned} p_{1,1}^{\text{eff}} &= \frac{1}{k} \text{tr} \left[\epsilon^T P^T (\tilde{D}_{\text{MB}}^{\text{SF}})^{-1} D_{\text{PV}} P \epsilon \right. \\ &\quad \left. \times \epsilon^T P^T \left\{ -(\tilde{D}_{\text{PV}})^{-1} \frac{\partial \tilde{D}_{\text{PV}}}{\partial \eta} \tilde{D}_{\text{PV}}^{-1} \tilde{D}_{\text{MB}}^{\text{SF}} + (\tilde{D}_{\text{PV}})^{-1} \frac{\partial \tilde{D}_{\text{MB}}^{\text{SF}}}{\partial \eta} \right\} P \epsilon \right]. \end{aligned} \quad (5.3.3)$$

To simplify $p_{1,1}$ and $p_{1,1}^{\text{eff}}$, I introduce two matrices, \mathcal{A} and \mathcal{B} , defined by

$$\mathcal{A} = P^T (\tilde{D}_{\text{MB}}^{\text{SF}})^{-1} \tilde{D}_{\text{PV}} P, \quad (5.3.4)$$

$$\mathcal{B} = P^T \left\{ (\tilde{D}_{\text{PV}})^{-1} \frac{\partial \tilde{D}_{\text{MB}}^{\text{SF}}}{\partial \eta} - (\tilde{D}_{\text{PV}})^{-1} \frac{\partial \tilde{D}_{\text{PV}}}{\partial \eta} (\tilde{D}_{\text{PV}})^{-1} \tilde{D}_{\text{MB}} \right\} P. \quad (5.3.5)$$

Using the relation $PP^T = 1$, $p_{1,1}^{\text{eff}}$ is rewritten as

$$p_{1,1} = \frac{1}{k} \text{Tr} [\mathcal{A}\mathcal{B}], \quad (5.3.6)$$

$$p_{1,1}^{\text{eff}} = \frac{1}{k} \text{tr} [(\epsilon^T \mathcal{A} \epsilon) (\epsilon^T \mathcal{B} \epsilon)]. \quad (5.3.7)$$

After employing matrix algebra in the five-dimensional notation ², we obtain

$$\mathcal{A} = \left(\begin{array}{c|c} \mathcal{A}_{11} & 0 \\ \hline \vec{\mathcal{A}}_1 & \mathbf{I} \end{array} \right), \quad \mathcal{A}_{11} = 1 - (1 - m_f)\mathring{\mathcal{A}}_{11} \quad (5.3.9)$$

$$\mathcal{B} = \left(\begin{array}{c|c} \mathcal{B}_{11} & 0 \\ \hline \vec{\mathcal{B}}_1 & \mathbf{0} \end{array} \right), \quad (5.3.10)$$

where $\mathcal{A}_{11}(\mathring{\mathcal{A}}_{11})$ and \mathcal{B}_{11} are four-dimensional operators, $\vec{\mathcal{A}}_1$ and $\vec{\mathcal{B}}_1$ are five-dimensional vectors with $N_5 - 1$ (whose elements are the four-dimensional operators) and \mathbf{I} and $\mathbf{0}$ are the identity and zero matrices with $(N_5 - 1) \times (N_5 - 1)$, respectively. Their explicit forms of $\mathcal{A}_{11}, \mathring{\mathcal{A}}_{11}, \mathcal{B}_{11}, \vec{\mathcal{A}}_1$ and $\vec{\mathcal{B}}_1$ are not required in the proof.

Substituting Eqs. (5.3.9) and (5.3.10) into Eq. (5.3.6), we obtain

$$\begin{aligned} p_{1,1} &= \frac{1}{k} \text{Tr} \left[\left(\begin{array}{c|c} \mathcal{A}_{11} & 0 \\ \hline \vec{\mathcal{A}}_1 & \mathbf{I} \end{array} \right) \left(\begin{array}{c|c} \mathcal{B}_{11} & 0 \\ \hline \vec{\mathcal{B}}_1 & \mathbf{0} \end{array} \right) \right] \\ &= \frac{1}{k} \text{tr} [\mathcal{A}_{11} \mathcal{B}_{11}], \end{aligned} \quad (5.3.11)$$

where the trace in the last line is now taken only on the four-dimensional lattice, color and spinor indices.

Similarly, substituting Eqs. (5.3.9) and (5.3.10) into Eq. (5.3.7), we obtain

$$\begin{aligned} p_{1,1}^{\text{eff}} &= \frac{1}{k} \text{Tr} \left[(1 \ 0 \ \cdots \ 0) \left(\begin{array}{c|c} \mathcal{A}_{11} & 0 \\ \hline \vec{\mathcal{A}}_1 & \mathbf{I} \end{array} \right) \begin{pmatrix} 1 \\ 0 \\ \vdots \\ 0 \end{pmatrix} (1 \ 0 \ \cdots \ 0) \left(\begin{array}{c|c} \mathcal{B}_{11} & 0 \\ \hline \vec{\mathcal{B}}_1 & \mathbf{0} \end{array} \right) \begin{pmatrix} 1 \\ 0 \\ \vdots \\ 0 \end{pmatrix} \right] \\ &= \frac{1}{k} \text{tr} [\mathcal{A}_{11} \mathcal{B}_{11}]. \end{aligned} \quad (5.3.12)$$

Thus, we have shown that $p_{1,1} = p_{1,1}^{\text{eff}}$.

²I note that

$$(D_q)^{-1} = \epsilon^T P^T (D_{\text{MB}})^{-1} D_{\text{PV}} P \epsilon, \quad (5.3.8)$$

holds true even with the SF boundary term.

Chapter 6

Numerical results

According to the last section, the MDWF with the SF boundary term satisfies the discrete symmetries required by the universality argument. The universality argument is written in the four-dimensional lattice field, and so we should check the anti-commutation relation between γ_5 and the propagator of the effective four-dimensional operator obtained from Eq. (5.1.7). As seen in Section 5.1, we cannot obtain the explicit form of D_q and the propagator, $S_q \equiv (D_q)^{-1}$. Thus the consistency between the SF scheme for the Dirac fermion and that for the MDWF has to be checked numerically. In the SF scheme, the following properties are known: the lowest eigenvalues of the Hermitian operator of the Dirac fermion, the time dependence for the propagator and the one-loop beta function of the renormalization group of QCD.

In this Chapter, I show the numerical analysis of the properties of the MDWFs in the SF scheme up to the one-loop level and compare these properties to those in the continuum SF theory. Without the background field, the propagator and lower eigenvalues of the Hermitian operator are solved analytically, which assists in confirming the universality of the MDWF proposed for the SF scheme in this thesis. The universality of the MDWF in the SF scheme was examined using the parameter sets shown in Table 6.1. Here, ω_j is set so that $U(x)$ in Eq. (3.2.5), the sign approximation function, is within the approximation range. In general, the approximation range is set from the lowest- to the highest-eigenvalue of \mathcal{H}_ω , and these values will vary with a/L at a fixed N_5 (Appendix B). To include all eigenvalues of \mathcal{H}_ω in the approximation range, this work employed a wide approximation range, regardless of N_5 and the lattice size L/a . The error between the sign function and the quasi-optimal approximation function, $\delta_{\text{QZ}}^{N_5}$, is summarized in Table 6.2.

Table 6.1: The common parameter set.

Operator	Shamir DWF	Boriçi DWF	Optimal Shamir	Optimal Chiu
b_j, c_j	$b_j = 1, c_j = 0$	$b_j = c_j = 1$	$b_j = \frac{\omega_j+1}{2}, c_j = \frac{\omega_j-1}{2}$	$b_j = c_j = \omega_j$
m_0	1.5	1.0 1.5	1.0	1.0
The approximation range	-	-	[0.001 : 1.00]	[0.01 : 7.000]

Table 6.2: $\delta_{\text{QZ}}^{N_5}$ with $N_5 = 8, 16,$ and 32 .

Operator	Optimal Shamir			Optimal		
	8	16	32	8	16	32
$\delta_{\text{QZ}}^{N_5}$	≤ 0.091	≤ 0.00061	$\leq 4.3 \times 10^{-8}$	≤ 0.072	≤ 0.00039	$\leq 1.8 \times 10^{-8}$

For the calculations in this section, I use the operator in Eq. (5.1.10). In appendix B, the range where all eigenvalues are involved is summarized for each kernel type \mathcal{H}_ω as a function of a/L . In order to simplify the analysis on the optimal type MDWF, I focus on the cases with $N_5 = 8, 16$ and 32 in this thesis.

6.1 Properties of the effective four-dimensional operator of the MDWF

6.1.1 Unitarity of the effective four-dimensional operator

Based on the discussion regarding the Hermitian operator $\gamma_5 D$ in Ref. [39], the spectrum of D_q should be in the unit circle. The universality argument states that the lattice chiral fermion operator with the SF boundary condition should satisfy the discrete symmetries and break chiral symmetry at the temporal boundary as stated in Section 4.1. However, this argument does not completely determine the form of the lattice operator. In this subsection, I first ascertain the spectrum of D_q in the complex plane with $m_{\text{res}} = 0, N_5 = 8, N_S = N_T = 6$, as in Figure 6.1. If the operator satisfies the GW relation, the eigenvalues will be located on the solid line in this figure. The eigenvalues are all within the circle, and so I conclude that the four-dimensional effective operator with the MDWF actually does not satisfy the unitarity property of the sign function which is required for lattice chiral symmetry. Thus, the required condition for the four-dimensional effective operator in the SF scheme is satisfied.

6.1.2 Lattice chiral symmetry breaking in the SF scheme

In the SF scheme, the lattice Chiral fermion operator should not satisfy the GW relation completely. Based on the Lüscher's universality argument and Eqs. (4.1.1)-(4.1.3), this lattice fermion operator should violate the GW relation only at the temporal boundaries. The temporal location of the violation of the GW relation, was examined using the metric [41]

$$\delta(n_4, m_4) = \sum_{\text{color, spin}} \left| \{ \gamma_5, \tilde{D}_q(n_4, m_4) \} - 2\tilde{D}_q(n_4, m_4)\gamma_5\tilde{D}_q(n_4, m_4) \right|, \quad (6.1.1)$$

where $\tilde{D}_q(n_4, m_4)$ is the zero-momentum portion in the spatial direction of $D_q(n, m)$. $\delta(n_4, m_4)$ should be reduced in the bulk region in the time direction as N_5 becomes large, and $\delta(n_4, m_4)$ values were calculated based on the MDWF using fixed values of $N_S = N_T = 20$ and

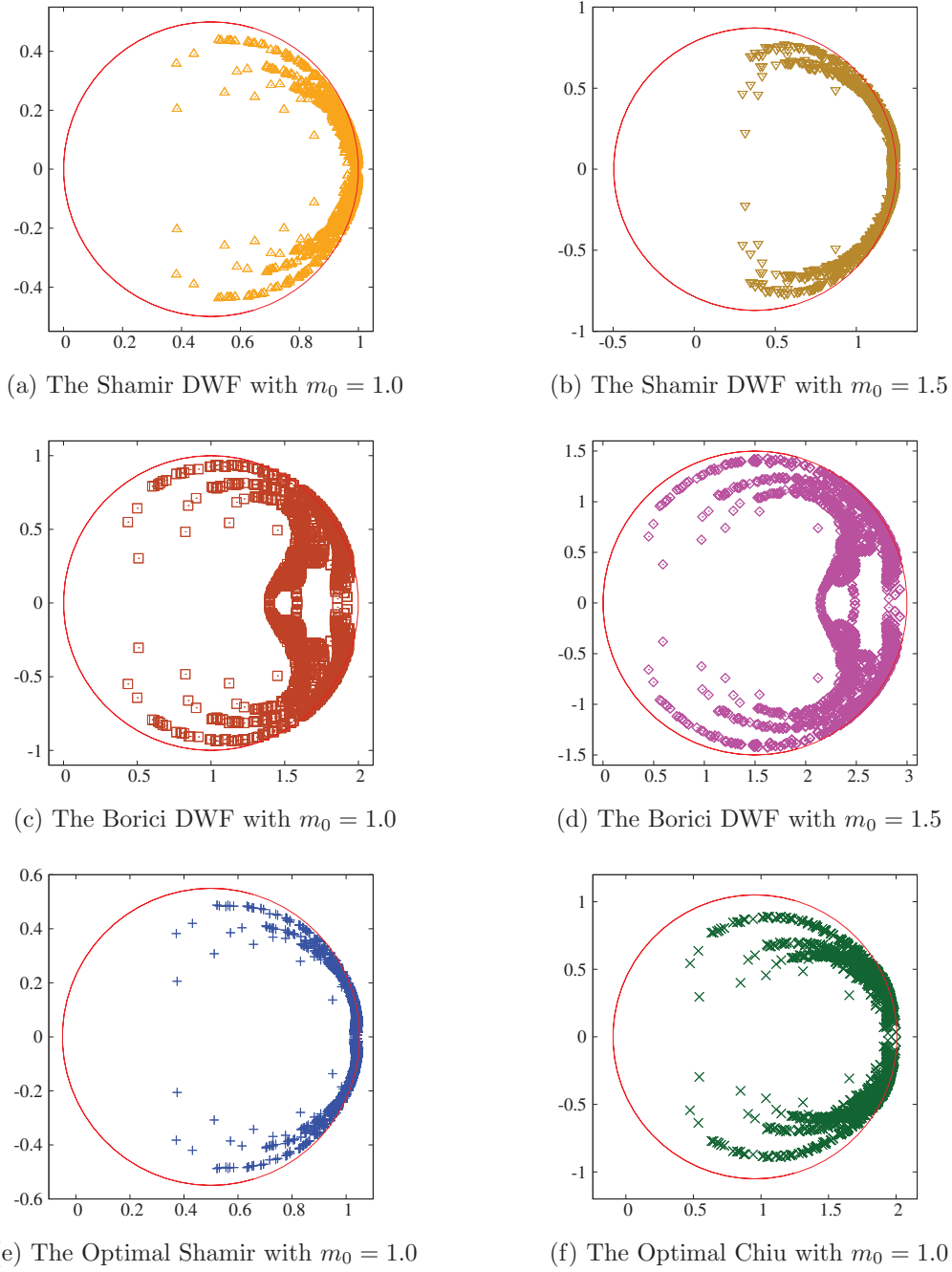


Figure 6.1: Unitary test

$N_5 = 8, 16$ and 32 to investigate the restoration and violation of the GW relation in Figs. 6.2-6.7.

In this figure, the axes represent the lattice indices in the time direction, n_4 and m_4 , and the magnitude of $\delta(n_4, m_4)$ is shown using a common log scale. For each MDWF with $N_5 = 8$, the violation of the GW relation remains in the bulk region. However, as we increase N_5 , the violation disappears from the bulk region, but remains at the temporal boundaries. I conclude that the MDWF in the SF scheme satisfies the property of the GW relation, as expected based on the universality argument.

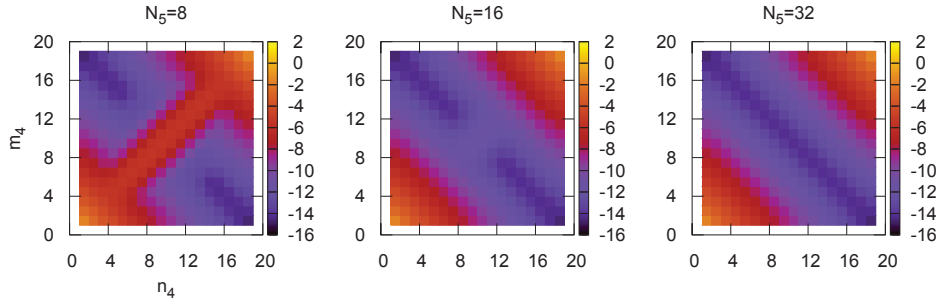


Figure 6.2: The GW relation breaking of the Shamir DWF with $m_0 = 1.0$.

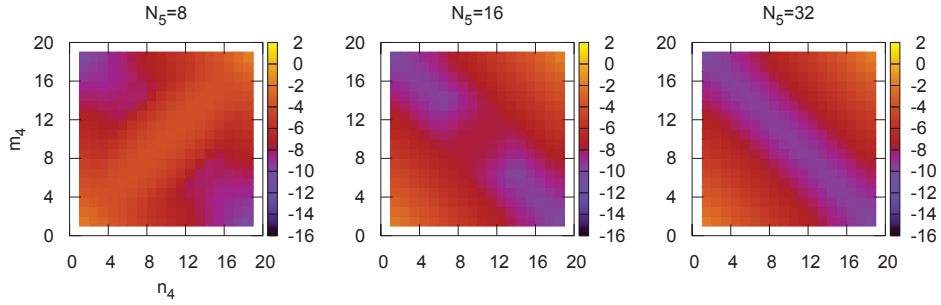


Figure 6.3: The GW relation breaking of the Shamir DWF with $m_0 = 1.5$.

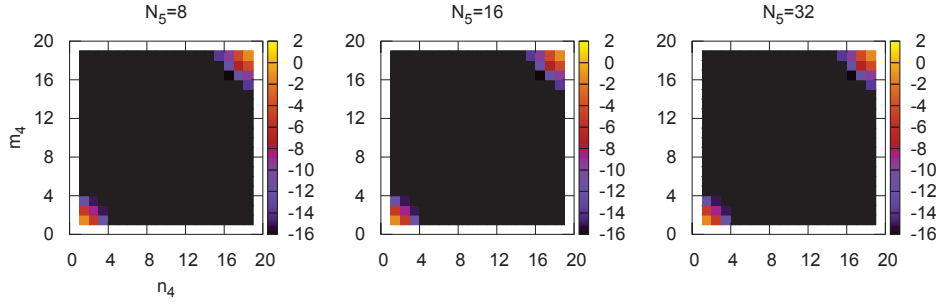


Figure 6.4: The GW relation breaking of the Borici DWF with $m_0 = 1.0$.

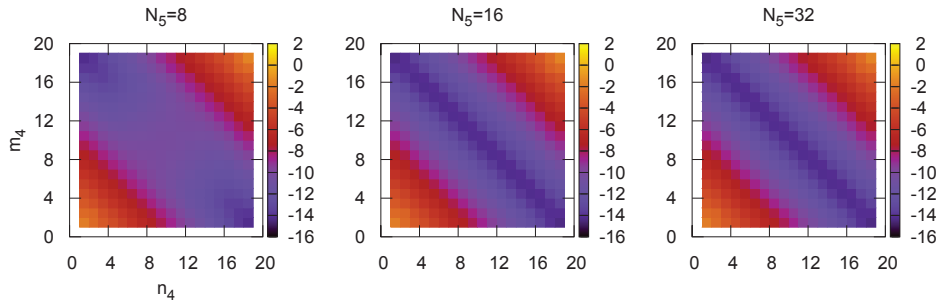


Figure 6.5: The GW relation breaking of the Borici DWF with $m_0 = 1.5$.

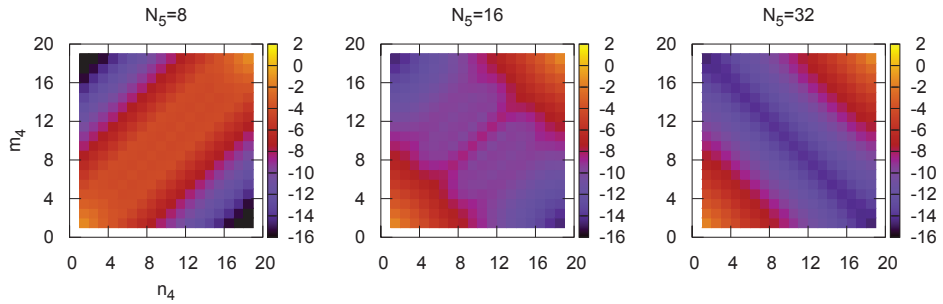


Figure 6.6: The GW relation breaking of the optimal Shamir DWF with $m_0 = 1.0$.

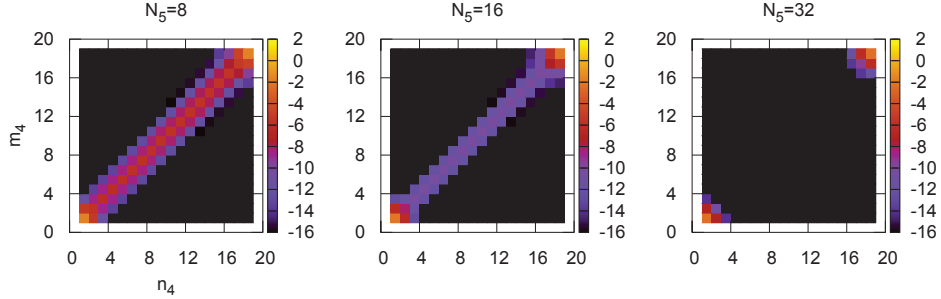


Figure 6.7: The GW relation breaking of the optimal Chiu DWF with $m_0 = 1.0$.

6.2 Universality check at the tree-level

6.2.1 Lowest eigenvalues of the Hermitian operator of the MDWFs

In this subsection, I investigate the eigenvalues of the effective four-dimensional operator, by computing the lowest ten eigenvalues with the MDWF and comparing these to the values in Ref. [28], generated using the continuum SF theory. Eigenvalues can be obtained analytically in the case of a vanishing background gauge field in the SF scheme, and those having a non-zero classical background field can be computed numerically, as in Ref. [57].

Figs. 6.8 and 6.9 show the cutoff dependence of the eigenvalues, $L^2 \tilde{D}_q^\dagger \tilde{D}_q$, with and without the classical background field. In these figures, the solid circles indicate those eigenvalues obtained analytically in Ref. [28]. Figure 6.8 shows eigenvalues without the background field have degeneracy in terms of the color index. In the case of a large lattice cutoff, the eigenvalues deviate from those in the continuum theory, although the eigenvalues eventually converge to the continuum limit. The continuum limits of the eigenvalues for $N_5 = 16$ and 32 were examined and the eigenvalues were found to agree at the continuum limit. If N_5 is small, the residual mass m_{res} has a finite value, and so renormalization for the tree-level is required. I conclude that the MDWF operator with the SF scheme realizes the massless Dirac fermion operator at the continuum limit for the tree-level.

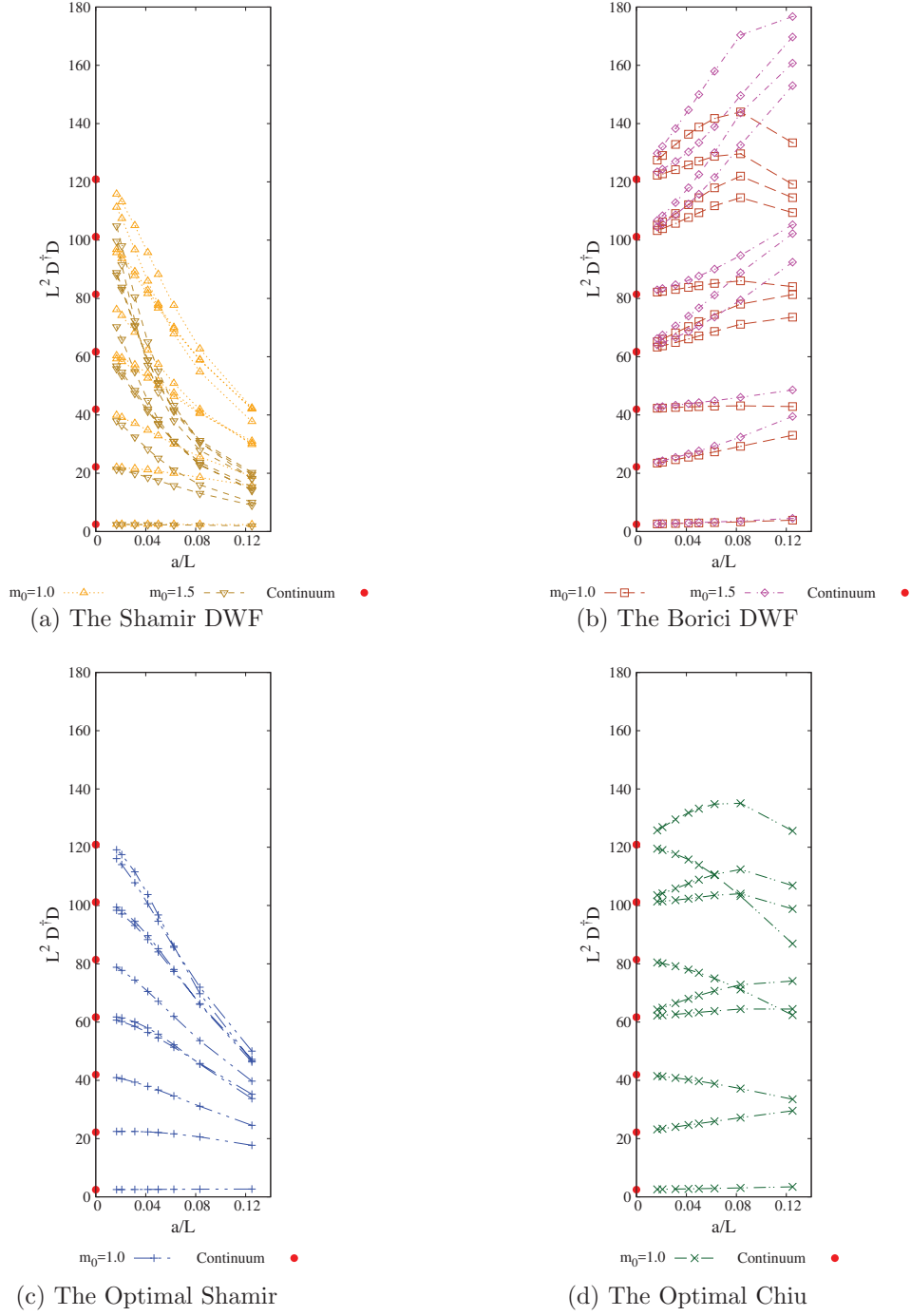


Figure 6.8: Lowest eigenvalues of hermitian operator of the MDWFs with $N_5 = 8$ and $c_{SF} = 1.0$ and the background field is not set.

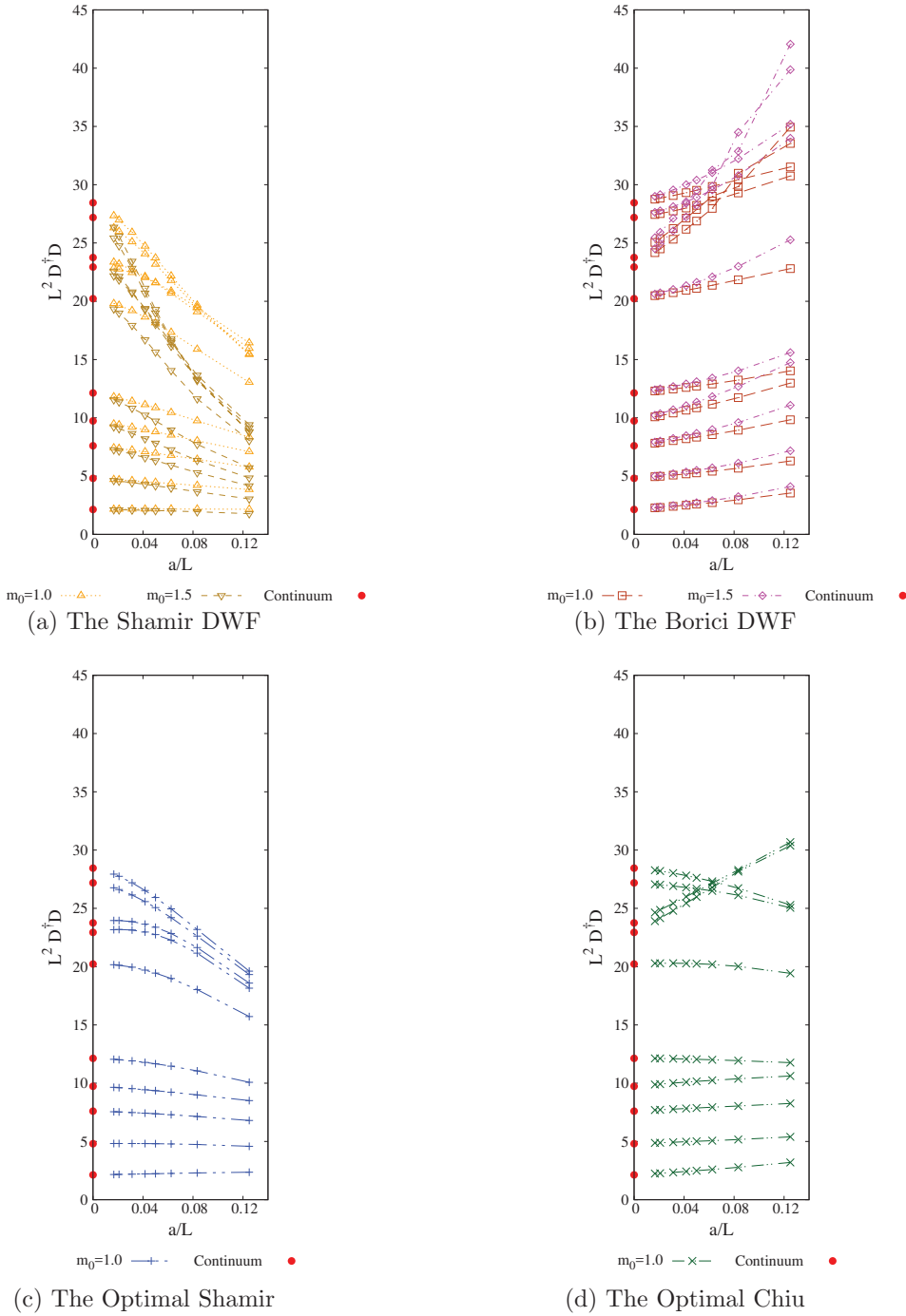


Figure 6.9: Lowest ten eigenvalues of hermitian operator of the MDWFs with $N_5 = 8$ and $c_{SF} = 1.0$.

6.2.2 Snapshot of the spin components of the MDWF propagator

In this subsection, I investigate the universality of the lattice Dirac propagator by directly comparing it with that in continuum theory. To do so, the $O(a)$ error coming from the boundary term, B_{SF} , in the lattice operator was removed by tuning c_{SF} using the PCAC relation. This improvement is discussed in Subsection 6.2.3.

In continuum theory, the Dirac propagator for the SF scheme is solved analytically [28, 69]. As an example, the SF Dirac operator without the classical background field in Eq. (2.1.9) is given by

$$\begin{aligned}
 S(x, y) &= (-\not{\partial}_x + m)G(x, y) = \frac{1}{L^3} \sum_{\mathbf{p}} \tilde{S}(\mathbf{p}, x_4, y_4) e^{i\mathbf{p}\cdot(\mathbf{x}-\mathbf{y})}, \\
 G(x, y) &= \frac{1}{L^3} \sum_{\mathbf{p}} \frac{e^{i\mathbf{p}\cdot(\mathbf{x}-\mathbf{y})}}{2E} \\
 &\times \left[\{ (e^{-E|x_4-y_4|} - e^{-E|x_4+y_4|}) (1 - \rho(E)) - (e^{E|x_4-y_4|} - e^{E|x_4+y_4|}) \rho(E) \} P_- \right. \\
 &\quad \left. + \{ (e^{-E|x_4-y_4|} - e^{-E|x_4+y_4-2T|}) (1 - \rho(E)) - (e^{E|x_4-y_4|} - e^{E|x_4+y_4-2T|}) \rho(E) \} P_+ \right],
 \end{aligned} \tag{6.2.1}$$

$$\tag{6.2.2}$$

where E is the energy and $\rho(E)$ is the energy density, given by

$$E = \sqrt{\left(\frac{\mathbf{p}}{L}\right)^2 + m_f^2}, \quad \rho(E) = \frac{ET - m_f T}{(ET + m_f T)e^{2ET} + (ET - m_f T)}. \tag{6.2.3}$$

Here, \mathbf{p} is the spatial momentum. At this point, the parameters are fixed such that $\mathbf{p} = \pi/(5L)$ and $m_f = 0$, so that we can obtain ET in a simple manner, as

$$ET = \frac{\sqrt{3}\pi T}{5L}. \tag{6.2.4}$$

The continuum limit of the propagator for the MDWF was studied and consistency with the Dirac propagator in Eq. (6.2.1) was examined. I defined the propagator of the MDWFs in the SF scheme from Eq. (5.1.10), as

$$\tilde{S}_q = (\tilde{D}_q)^{-1} = Z \tilde{D}_{\text{eff}}^{-1}(m_{cr}), \tag{6.2.5}$$

and calculated $\tilde{S}_q(x_4, y_4)$, where $x_4 = an_4, y_4 = am_4$, while varying source position and the number of time dimensional indices. In these calculations, \mathbf{p} was defined by $\mathbf{p} = (2\pi\mathbf{n} + \boldsymbol{\theta})/N_s$, and the parameters fixed as $\mathbf{n} = \mathbf{0}, \boldsymbol{\theta} \equiv (\theta_1, \theta_2, \theta_3) = (\pi/5, \pi/5, \pi/5)$ and $m_{\text{res}} = 0$, to compare with the Dirac propagator based on the conditions associated with Eq. (6.2.4). Figs. 6.10 and 6.11 present the time dependence of the propagator $S(x_4, y_4)$ for the Shamir DWF and the Boriçi DWF with $m_f = 0$ and the source at $y_4 = 0$ for each spin-component tabulated in 4×4 form. Here, $m_0 = 1.0, N_S = N_T = 50, N_5 = 16$ and $c_{\text{SF}} = 1.0$. The solid line (*Continuum*) indicates the Dirac propagator in the continuum theory Eq. (6.2.1), while the up-triangles

(*SDWF*) and the boxes (*BDWF*) indicate values obtained using the Shamir DWF and Boriçi DWF, respectively. The propagator obtained with the Shamir DWF is consistent with that for continuum theory, what there are large deviations in the case of the propagator generated using the Boriçi DWF.

I also assessed the time dependence of the propagator $\tilde{S}_q(x_4, y_4)$ with the source at $y_4 = a$ (Figs. 6.12 and 6.13). In these calculations, the parameters were set to be equal to those used to generate the values in Figs. 6.10 and 6.11. Comparing these figures, a discrepancy is evident between the propagators for the SF continuum and the lattice SF Dirac operators is sorely at the temporal boundaries. This discrepancy at the temporal boundaries has been previously suggested for the overlap fermion [42]. I subsequently investigated the origin of the gap that appeared when using the MDWF in certain studies, based on the continuum limit of the propagator.

Figs. 6.10-6.13 were used to determine the continuum limit of certain spin components of the propagator $S_{\text{MB}}(x_4, y_4)_{i_s, j_s}$ with the source at $y_4 = 0$, where i_s and j_s are spin components. Table 6.3 summarizes the relative discrepancy of the propagators of the continuum Dirac fermion and the MDWF for $N_T = 10, 20$ and 40 . The relative discrepancy is defined by

$$f_{\text{Re}}(x_4, i_s, j_s) = \left| \frac{\text{Re}(S_{\text{MB}}(x_4, 0)_{i_s, j_s}) - \text{Re}(S(x_4, 0)_{i_s, j_s})}{\text{Re}(S(x_4, 0)_{i_s, j_s})} \right|, \quad (6.2.6)$$

$$f_{\text{Im}}(x_4, i_s, j_s) = \left| \frac{\text{Im}(S_{\text{MB}}(x_4, 0)_{i_s, j_s}) - \text{Im}(S(x_4, 0)_{i_s, j_s})}{\text{Im}(S(x_4, 0)_{i_s, j_s})} \right|. \quad (6.2.7)$$

Here, $f_{\text{Re}}(x_4, i_s, j_s)$ and $f_{\text{Im}}(x_4, i_s, j_s)$ of the Shamir DWF approach zero at the continuum limit, while the values for the Boriçi DWF remain at approximately 0.57. From Table 6.3 it is apparent that the gap in the propagators between the MDWF and Dirac fermions is related to the Möbius parameters.

Table 6.3: The continuum limits of the relative ratios of the propagators. The propagators are calculated with $N_5 = 4$.

Möbius parameters	$b_j = 1, c_j = 0$			$b_j = 1, c_j = 1$		
	10	20	50	10	20	50
$f_{\text{Re}}(T - a, 1, 1)$	0.0806327	0.0419331	0.0171213	0.527432	0.551698	0.567316
$f_{\text{Re}}(a, 3, 1)$	0.0315943	0.0185479	0.0080075	0.569639	0.571646	0.575014
$f_{\text{Re}}(a, 4, 2)$	0.0315943	0.0185479	0.0080075	0.569639	0.571646	0.575014
$f_{\text{Im}}(a, 4, 1)$	0.0315943	0.0185479	0.0080075	0.569639	0.571646	0.575014
$f_{\text{Im}}(a, 3, 2)$	0.0315943	0.0185479	0.0080075	0.569639	0.571646	0.575014

Figure 6.10: Real part of $S(x_4, y_4 = 0)$ with $m_f = 0.0$

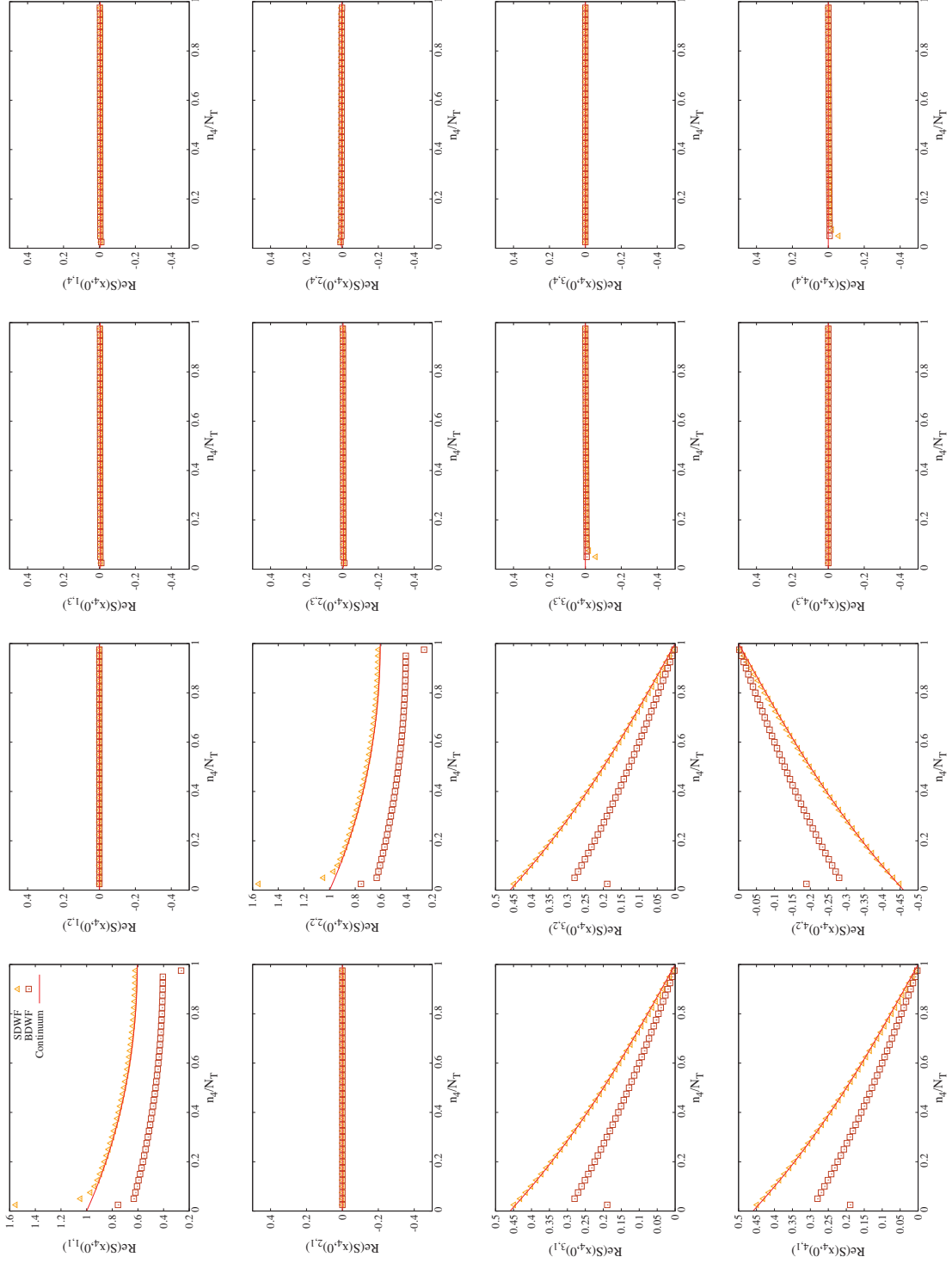


Figure 6.11: Imaginary part of $S(x_4, y_4 = 0)$ with $m_f = 0.0$

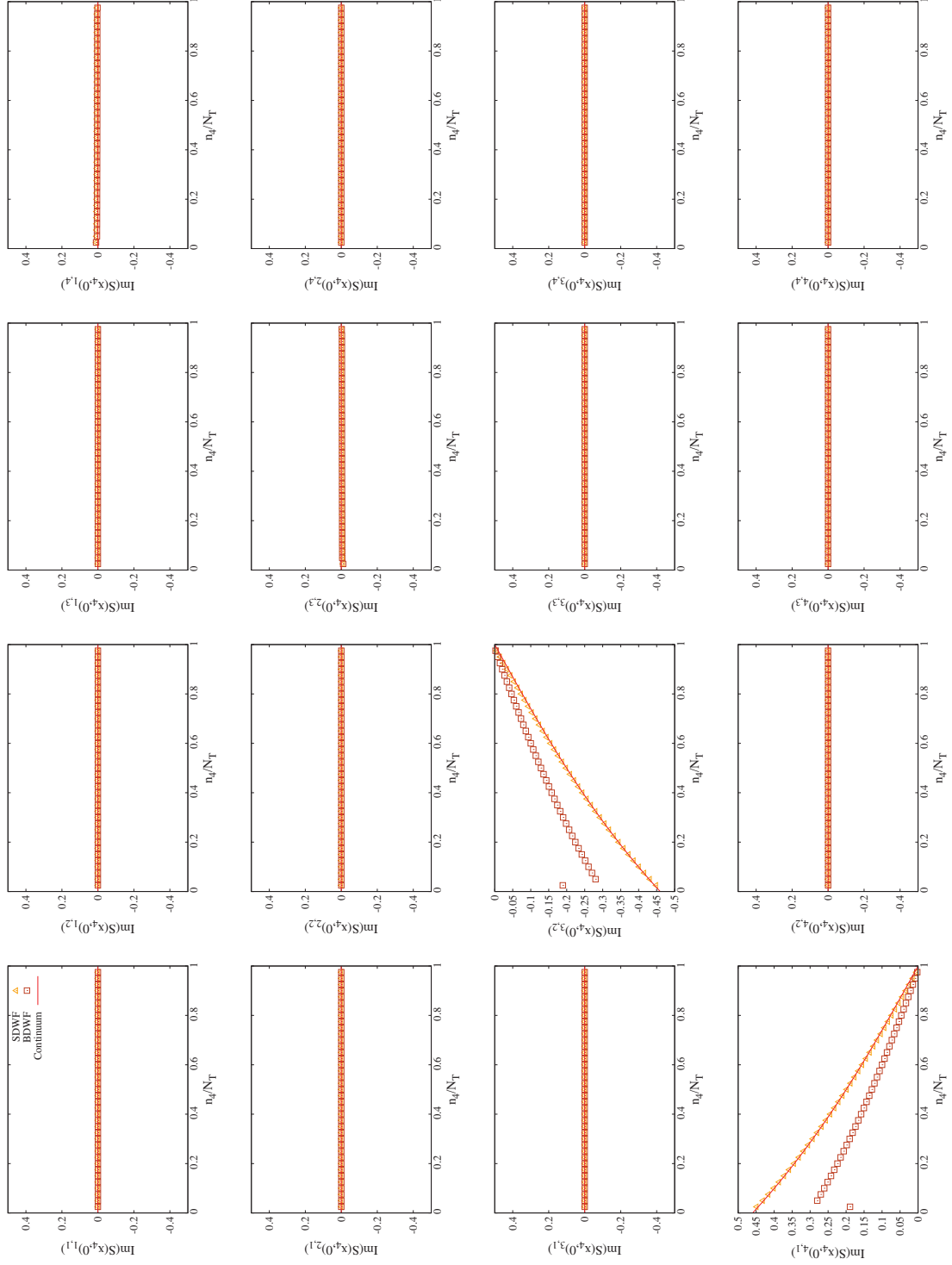


Figure 6.12: Real part of $S(x_4, y_4 = a)$ with $m_f = 0.0$

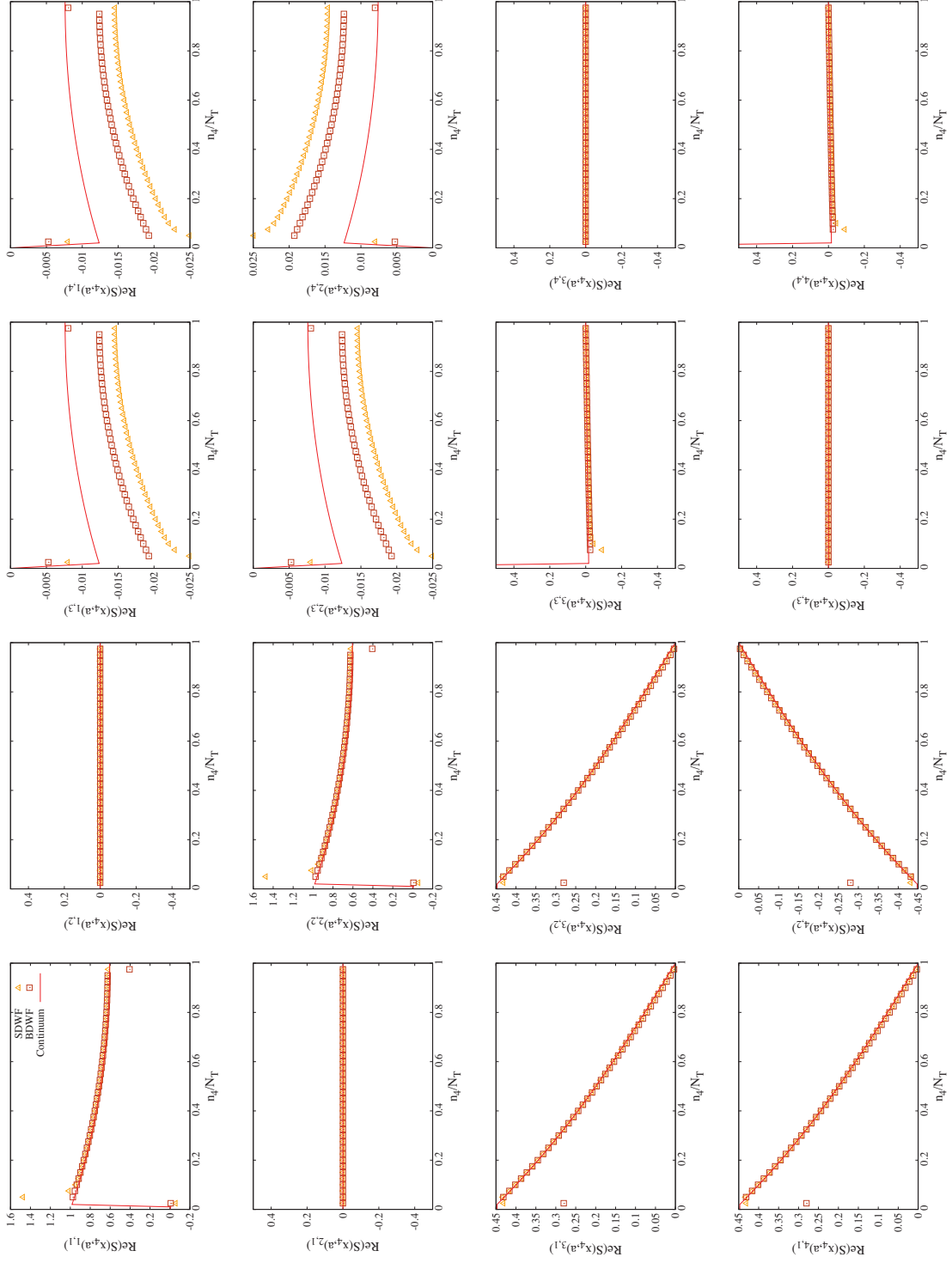
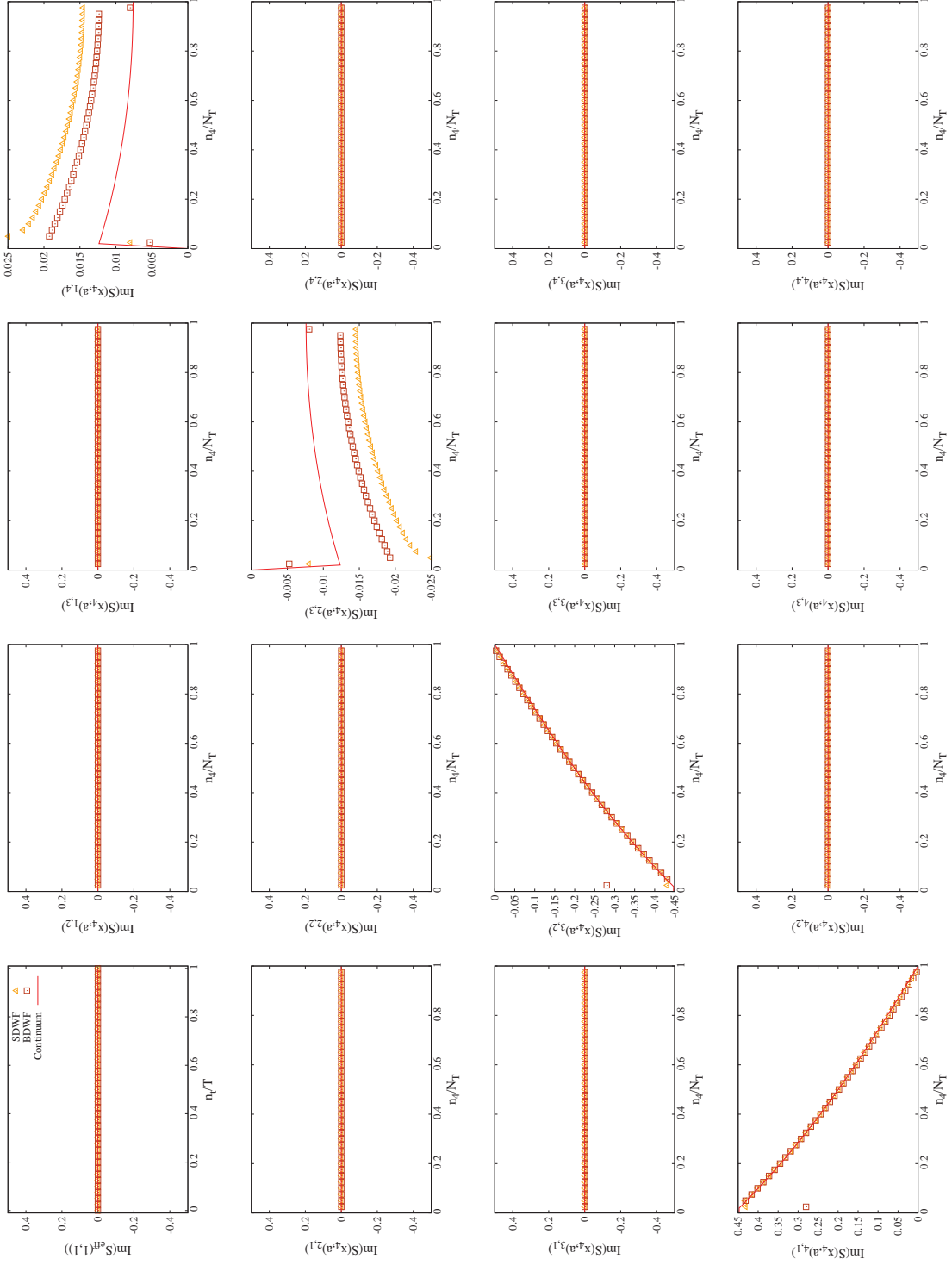
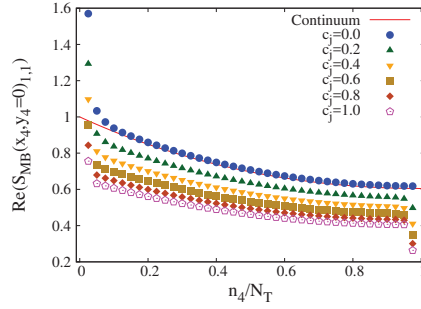


Figure 6.13: Imaginary part of $S(x_4, y_4 = a)$ with $m_f = 0.0$.




 Figure 6.14: Time dependence of the propagator $S_{\text{MB}}(x_4, y_4 = 0)_{1,1}$.

I further investigate the propagator of the MDWF varying the Möbius parameter c_j . Figure 6.14 shows the time dependence of the propagator $\tilde{S}_q(x_4, y_4 = 0)_{1,1}$ for various values of c_j . The parameters were set to $N_S = N_T = 50$, $m_0 = 1.0$, $m_{\text{res}} = 0.0$, and $N_5 = 4$. The solid line in this figure corresponds to the propagator in continuum theory, while the data points show the propagator of the MDWF with the Möbius parameters $b_j = 1$ and certain values of c_j . Data labeled $c_j = 0$ correspond to the propagator of the Shamir DWF, which agrees only with the Dirac propagator at the continuum limit. Propagators with finite values of c_j do not agree with that in the continuum theory. The ratio of the propagators becomes a common constant value in the continuum limit regardless of the existence of the background field and the color index [56]. I conclude that this gap is constant and occurs at the time boundary in cases with finite values for c_j . This phenomenon has been observed for the overlap fermion and investigated in [42, 56]. The resolution to remove the deviation in the propagators at the temporal boundaries with $c_j \neq 0$ is to renormalize the temporal boundary fields [42, 56].

The temporal boundary field is defined by the following three-dimensional fields in the continuum theory as

$$P_+ \psi(x)|_{x_4=0} = \rho(\mathbf{x}), \quad P_- \psi(x)|_{x_4=T} = \rho'(\mathbf{x}), \quad (6.2.8a)$$

$$\bar{\psi}(x)P_-|_{x_4=0} = \bar{\rho}(\mathbf{x}), \quad \bar{\psi}(x)P_+|_{x_4=T} = \bar{\rho}'(\mathbf{x}), \quad (6.2.8b)$$

$$\zeta(\mathbf{x}) = P_- \psi(x)|_{x_4=0}, \quad \zeta'(\mathbf{x}) = P_+ \psi(x)|_{x_4=T}, \quad (6.2.9a)$$

$$\bar{\zeta}(\mathbf{x}) = \bar{\psi}(x)P_+|_{x_4=0}, \quad \bar{\zeta}'(\mathbf{x}) = \bar{\psi}(x)P_-|_{x_4=T}. \quad (6.2.9b)$$

In lattice field theory, the lattice version of Eq. (6.2.8) cannot be defined but Eq. (6.2.9) can be defined as

$$\hat{\zeta}(\mathbf{n}) = U_4(n - \hat{4})P_- \hat{\psi}(n)|_{n_4=1}, \quad \hat{\zeta}'(\mathbf{n}) = U_4(n)^\dagger P_+ \hat{\psi}(n)|_{n_4=N_T-1}, \quad (6.2.10a)$$

$$\hat{\bar{\zeta}}(\mathbf{n}) = \hat{\bar{\psi}}(n)P_+ U_4(n - \hat{4})^\dagger|_{n_4=1}, \quad \hat{\bar{\zeta}}'(\mathbf{n}) = \hat{\bar{\psi}}(n)P_- U_4(n)|_{n_4=N_T-1}. \quad (6.2.10b)$$

The form of the lattice boundary fields Eq. (6.2.10) is the simplest one and usually used in the Wilson-type fermions. The same form is also used for the DWF and the overlap

fermion [39, 40, 41]. I proposed an extended form for the boundary operators in Ref. [56]. The extended boundary operators are defined by

$$\begin{aligned}\hat{\zeta}(\mathbf{n}) &= U_4(n - 2 \cdot \hat{4})U_4(n - \hat{4})P_- \hat{\psi}(n)|_{n_4=2}, \\ \hat{\zeta}'(\mathbf{n}) &= U_4(n + \hat{4})^\dagger U_4(n)^\dagger P_+ \hat{\psi}(n)|_{n_4=N_T-2},\end{aligned}\tag{6.2.11a}$$

$$\begin{aligned}\tilde{\zeta}(\mathbf{n}) &= \tilde{\psi}(x)P_+ U_4(n - \hat{4})^\dagger U_4(n - 2 \cdot \hat{4})^\dagger|_{n_4=2}, \\ \tilde{\zeta}'(\mathbf{n}) &= \tilde{\psi}(n)P_- U_4(n)U_4(n + \hat{4})|_{n_4=N_T-2}.\end{aligned}\tag{6.2.11b}$$

Using the temporal boundary field in Eq. (6.2.11), we find that the discrepancy of the propagator between the MDWF and the Dirac fermion vanishes and the consistency of the MDWF with $c_j \neq 0$ to the continuum theory is recovered. From these observations, I conclude that the propagators of the MDWF with various parameters are all consistent with that of the continuum theory in the continuum limit, which strongly supports the validity of the MDWF with the SF boundary operator Eq. (5.1.9) at least at the tree-level.

6.2.3 Tuning c_{SF} based on the PCAC relation

Although the operators satisfying the GW relation are automatically $O(a)$ improved, the operators in the SF scheme could incorporate the $O(a)$ error originating from the explicit breaking of lattice chiral symmetry at the boundary. The MDWF with the SF boundary actually incorporates the $O(a)$ error as a result of the additional term B_{SF} , although this can be removed by tuning the coefficient c_{SF} . To tune c_{SF} so as to improve $O(a)$, I employed the PCAC relation. In the lattice calculation, the correlation functions $f_A(n_4)$ and $f_P(n_4)$ are given by

$$f_A(n_4) = \frac{-1}{2N_S^3} \text{Tr} \left[\tilde{S}(n_4, 1)^\dagger P_+ \gamma_4 \tilde{S}(n_4, 1) P_+ \right],\tag{6.2.12}$$

$$f_P(n_4) = \frac{1}{2N_S^3} \text{Tr} \left[\tilde{S}(n_4, 1)^\dagger P_+ \tilde{S}(n_4, 1) P_+ \right],\tag{6.2.13}$$

where $\tilde{S}(n_4, m_4)$ is the zero-momentum projection of $S(n, m) = (D_q)^{-1}(n, m)$. From the PCAC relation in the continuum theory in Sec. 4.2, the ratio $f_A(T/2)/f_P(T/2)$ should agree with $-1/\cosh(2\sqrt{3}\theta)$ (Eq. (4.2.21)) at the continuum limit. In this work, $f_A(n_4)$ and $f_P(n_4)$ were calculated by varying a/L and c_{SF} with $\theta = \pi/5$ and $N_5 = 8, 16$ or 32 ¹.

Figure 6.15 represents the cutoff dependence of $f_A(T/2)/f_P(T/2)$ as calculated using the MDWF with $N_5 = 8$ and for $c_{\text{SF}} = 0.2, 0.4, 0.6$ or 0.8 . The solid circle at $a/L = 0$ is the ratio of the correlation functions in the SF continuum theory at $\theta = \pi/5$, $f_A(T/2)/f_P(T/2) = -0.22398042699$. For the Shamir DWF (Figs. 6.15(a) and 6.15(b)) and the Boriçi DWF (Figs. 6.15 (c) and 6.15(d)), the $f_A(T/2)/f_P(T/2)$ values agree with that obtained from

¹It is possible to tune c_{SF} with adjusting either $f_A(T/2)$ or $f_P(T/2)$ to the corresponding analytic forms in Eqs. (4.2.18) or (4.2.19). I use $f_A(T/2)/f_P(T/2)$ for the tuning of c_{SF} because of the simple form of $f_A(T/2)/f_P(T/2)$ as seen in Eq. (4.2.21).

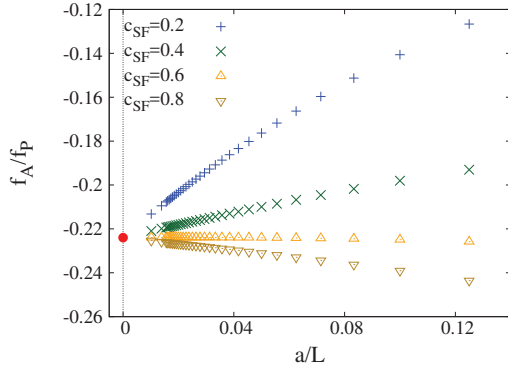
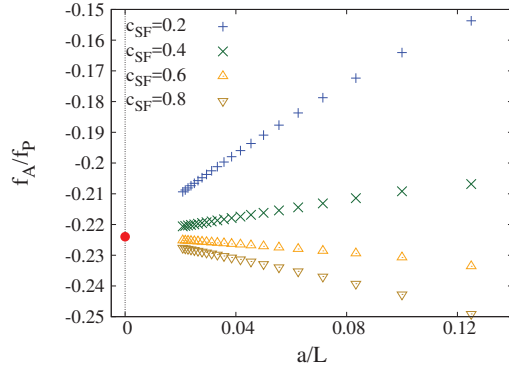
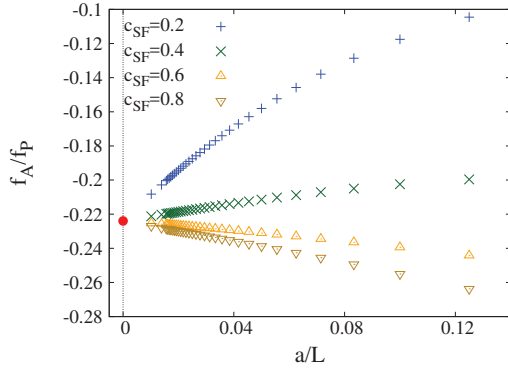
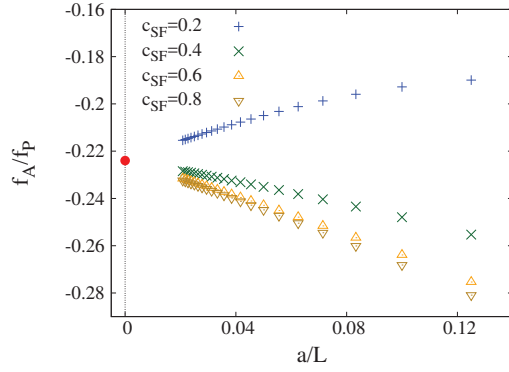
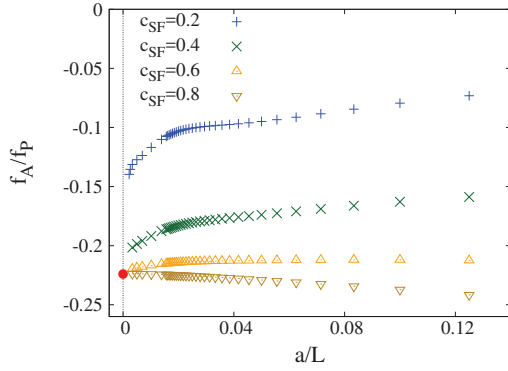
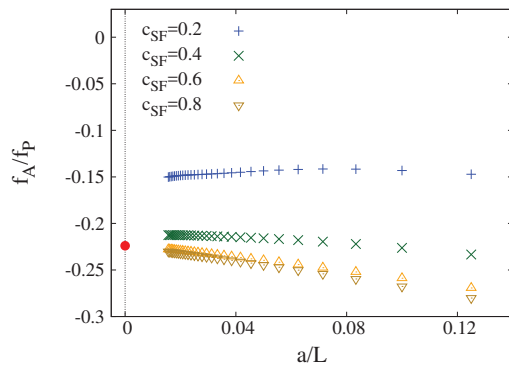

 (a) Shamir DWF with $m_0 = 1.0$

 (b) Shamir DWF with $m_0 = 1.5$

 (c) Borici DWF with $m_0 = 1.0$

 (d) Borici DWF with $m_0 = 1.5$

 (e) Optimal Shamir DWF with $m_0 = 1.0$

 (f) Optimal Chiu DWF with $m_0 = 1.0$

 Figure 6.15: The cutoff dependence with the ratio of $f_A(T/2)$ to $f_P(T/2)$.

continuum theory at the continuum limit. In the case of the optimal Shamir DWF and the optimal Chiu DWF, $f_A(T/2)/f_P(T/2)$ in association with a lower c_{SF} approaches the expected value over a narrow range of a/L . This unique behavior is seen only at a small N_5

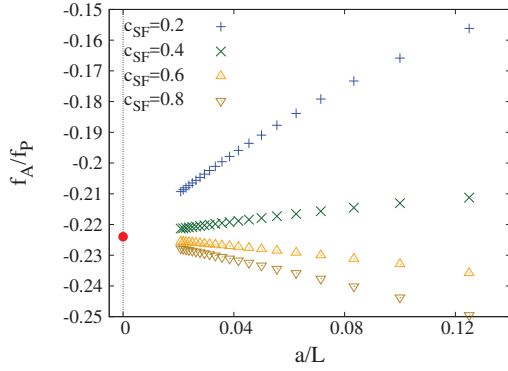
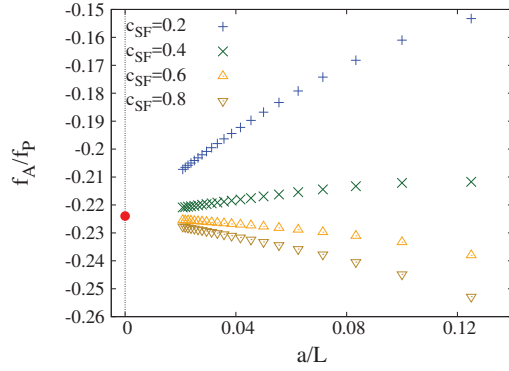
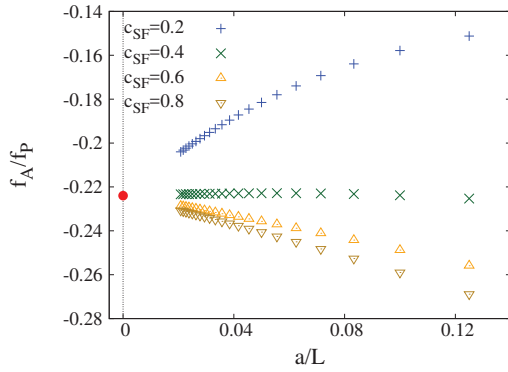
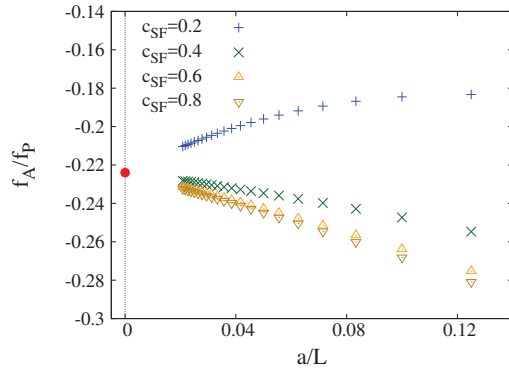
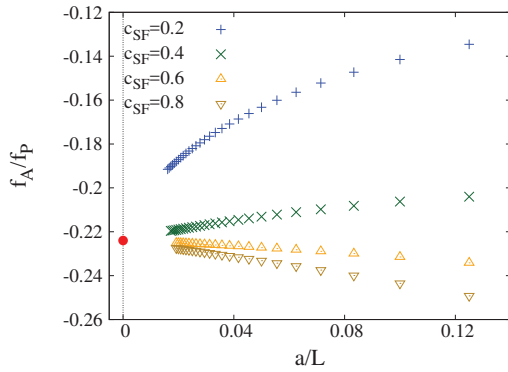
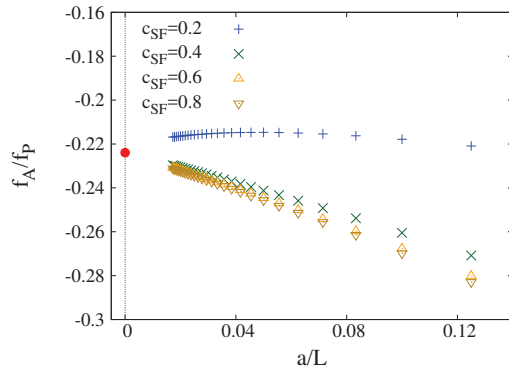

 (a) Shamir DWF with $m_0 = 1.0$

 (b) Shamir DWF with $m_0 = 1.5$

 (c) Borici DWF with $m_0 = 1.0$

 (d) Borici DWF with $m_0 = 1.5$

 (e) Optimal Shamir DWF with $m_0 = 1.0$

 (f) Optimal Chiu DWF with $m_0 = 1.0$

 Figure 6.16: The cutoff dependence with the ratio of $f_A(T/2)$ to $f_P(T/2)$.

and the ratios all approach the expected values as N_5 becomes greater (*c.f.* Figure 6.15). Moreover, $f_A(T/2)/f_P(T/2)$ varies with N_5 , which is not observed in the case of the Shamir and Borici DWFs. Hence, we must tune the c_{SF} values of the MDWF operator for each N_5 .

Here, c_{SF} was tuned by fitting $f_A(T/2)/f_P(T/2)$ for $N_5 = 32$, to avoid $O(a)$ discretization errors resulting from the explicit violation of lattice chiral symmetry at small values of N_5 . The accuracy of the chiral symmetry breaking for the MDWF operator was obtained by calculating the correlation function. In the lattice calculation, $f_A(T/2)/f_P(T/2)$ was expressed as a function of a/L and c_{SF} . In order to eliminate the $O(a)$ error from the boundary operator, I fit the lattice data and extracted the $O(a)$ contribution as a function of c_{SF} , then eliminated the error by tuning c_{SF} . The $O(a)$ error was extracted using the polynomial

$$\begin{aligned} f_A(T/2)/f_P(T/2) = & A_{00} + (A_{01} + A_{11}c_{\text{SF}} + A_{21}c_{\text{SF}}^2 + A_{31}c_{\text{SF}}^3)(a/L) \\ & + (A_{02} + A_{12}c_{\text{SF}} + A_{22}c_{\text{SF}}^2 + A_{32}c_{\text{SF}}^3)(a/L)^2 \\ & + (A_{03} + A_{13}c_{\text{SF}} + A_{23}c_{\text{SF}}^2 + A_{33}c_{\text{SF}}^3)(a/L)^3 + \dots \end{aligned} \quad (6.2.14)$$

where A_{00} was expected to be -0.22398042699 at $\theta = \pi/5$. I fitted $f_A(T/2)/f_P(T/2)$ as a multivariable function of c_{SF} and a/L with $A_{00} = -0.22398042699$. The $O(a)$ improvement was accomplished by determining c_{SF} through solving the equations

$$A_{01} + A_{11}c_{\text{SF}} + A_{21}c_{\text{SF}}^2 + A_{31}c_{\text{SF}}^3 = 0. \quad (6.2.15)$$

The resulting c_{SF} values for the MDWFs are summarized in Table 6.4.

Table 6.4: Values of c_{SF} for $O(a)$ improvement

Operator	Shamir		Boriçi		Optimal Shamir			Optimal Chiu		
	1.0	1.5	1.0	1.5	1.0			1.0		
m_0	1.0	1.5	1.0	1.5	1.0			1.0		
N_5	32		32		8	16	32	8	16	32
c_{SF}	0.5089	0.520	0.4167	0.312	0.820	0.630	0.5432	0.553	0.392	0.265

6.3 Universality at the one-loop level

To confirm consistency with QCD perturbation theory, I calculated $p_{1,1}$ in Eq. (5.3.1) for a set of parameters for the MDWF using $N_S = N_T$ while varying the lattice cutoff. In lattice calculations involving MDWFs, $p_{1,1}$ is calculated as

$$\begin{aligned} p_{1,1} &= \frac{1}{k} \frac{\partial}{\partial \eta} \left[\text{Tr} \ln \left[Z^{-1} D_{\text{PV}}^{-1} D_{\text{MB}}^{\text{SF}} \right] \right] \\ &= \frac{1}{k} \sum_{\mathbf{p}} \text{Tr} \left[\frac{\partial \tilde{D}_{\text{MB}}^{\text{SF}}}{\partial \eta} (\tilde{D}_{\text{MB}}^{\text{SF}})^{-1} - \frac{\partial \tilde{D}_{\text{PV}}}{\partial \eta} (\tilde{D}_{\text{PV}})^{-1} \right]. \end{aligned} \quad (6.3.1)$$

Here, $p_{1,1}$ depends on the lattice cutoff a/L and N_5 and is expanded asymptotically towards the continuum limit in the form of

$$p_{1,1} \approx \sum_{k=0}^{\infty} (A_k + B_k \ln L/a) \left(\frac{a}{L} \right)^k. \quad (6.3.2)$$

In the case of analysis at the one-loop level, it is helpful to consider the consistency of the coefficients A_0, B_0, A_1 , and B_1 , at the continuum limit. A_0 has a relationship between the SF and $\overline{\text{MS}}$ schemes and depends on the lattice actions, since it is computed with lattice regularization in the bare coupling expansion. As $N_5 \rightarrow \infty$, the Shamir and optimal Shamir DWF actions transition to the standard domain wall fermion action and the Boriçi and optimal Chiu DWF actions become the overlap fermion action. Values of A_0 for each lattice action are summarized in Table 6.5 [70]. B_0 is expected to have a universal value

 Table 6.5: The expected values of A_0

The lattice actions	m_0	The expectation value of A_0
The standard domain wall fermion actions	1.0	0.0010886(51)
	1.5	-0.0026362(33)
The overlap fermion actions	1.0	0.01118458(16)
	1.5	0.01191070(16)

corresponding to the one-loop beta function, $B_0 = 2b_{0,1} = -1/(12\pi^2) \simeq -0.00844343 \dots$. Thus, it is important to confirm the consistency of the fitting result for B_0 with the expected value.

The coefficients A_1 and B_1 represent the $O(a)$ error in the lattice regularization. When employing the classical background field, the quark propagator interacts with the background field, which has an $O(a)$ error. This error cannot be eliminated by the counter term of the lattice Dirac operator in the temporal boundary direction, but can be eliminated using the counter term of the gauge action for the temporal boundary [27, 29, 40, 41, 57]. A_1 can be removed by tuning the coefficient of the boundary counter term in the gauge action. In quantum field theory, the B_1 term is omitted in the perturbation theory because it vanishes in the continuum limit, however, comes out in lattice field theory as an $O(a)$ error. This occurs because the lattice chiral symmetry is not exact at finite values of N_5 when working with MDWFs, and so it is expected that B_1 will be minimal when N_5 is sufficiently large.

The value of $p_{1,1}$ was calculated for various values and combinations of N_5 , the lattice cutoff and Möbius parameters. I determined values for A_0, B_0, A_1 and B_1 from $p_{1,1}$ using the following procedures.

1. B_0 by the free-fitting of Eq (6.3.2)
2. A_0 by the constrained fitting of Eq (6.3.2) with fixed $B_0 = 2b_{0,1}$.
3. B_1 by the constrained fitting of Eq (6.3.2) with fixed $B_0 = 2b_{0,1}$ and A_0 .
4. A_1 by the constrained fitting of Eq (6.3.2) with fixed $B_0 = 2b_{0,1}$ and A_0 .

6.3.1 Fitting results

The consistency with B_0 was assessed by free-fitting using the expansion form of $p_{1,1}$, as

$$p_{1,1} = (A_0 + B_0 \ln(L/a)) + (A_1 + B_1 \ln(L/a)) \left(\frac{a}{L}\right), \quad (6.3.3)$$

while varying the fitting range. The best fitting results for B_0 are shown in Tabs. 6.6-6.10. Here, the A_0 and B_0 values for $N_5 = \infty$ are the theoretically expected values based on consistency. Only values that represented fitting results for B_0 were included in these tables, but it is evident that A_0 approaches the expected value based on continuum theory. The coefficient B_1 is very close to zero at $N_5 = 32$, which is expected in the case of a sufficiently large N_5 as chiral symmetry is restored, except for the Boriçi DWF with $m_0 = 1.5$.

 Table 6.6: The Shamir DWF with $m_0 = 1.5$.

N_5	8	16	32	∞
Fit range	$18 \leq L/a \leq 48$	$26 \leq L/a \leq 48$	$28 \leq L/a \leq 48$	-
A_0	-0.00376(6)	-0.002666(19)	-0.002615(15)	-0.0026362(33)
B_0	-0.008430(11)	-0.008440(3)	-0.008443(3)	-0.00844343
A_1	0.0315(4)	0.02335(19)	0.02316(16)	-
B_1	-0.0047(3)	-0.00216(12)	-0.00220(10)	-
$\chi^2/\text{d.o.f}$	1.48×10^{-7}	1.05×10^{-8}	5.53×10^{-9}	-

 Table 6.7: The Boriçi DWF with $m_0 = 1.0$.

N_5	8	16	32	∞
Fit range	$18 \leq L/a \leq 48$	$22 \leq L/a \leq 48$	$22 \leq L/a \leq 48$	-
A_0	0.01015(24)	0.0113(3)	0.0115(3)	0.01118458(16)
B_0	-0.008318(44)	-0.00847(5)	-0.00852(5)	-0.00844343
A_1	-0.0321(17)	-0.029(2)	-0.026(2)	-
B_1	0.0087(13)	0.0039(15)	0.0020(15)	-
$\chi^2/\text{d.o.f}$	6.11×10^{-7}	3.18×10^{-7}	3.12×10^{-7}	-

 Table 6.8: The Boriçi DWF with $m_0 = 1.5$.

N_5	8	16	32	∞
Fit range	$16 \leq L/a \leq 80$	$34 \leq L/a \leq 48$	$10 \leq L/a \leq 48$	-
A_0	0.01056(19)	0.0118(3)	0.0145(12)	0.01191070(16)
B_0	-0.008268(33)	-0.00846(5)	-0.0088(2)	-0.00844343
A_1	-0.0504(18)	-0.057(3)	0.019(5)	-
B_1	0.0149(12)	0.011(2)	-0.024(5)	-
$\chi^2/\text{d.o.f}$	2.67×10^{-6}	2.45×10^{-8}	1.43×10^{-5}	-

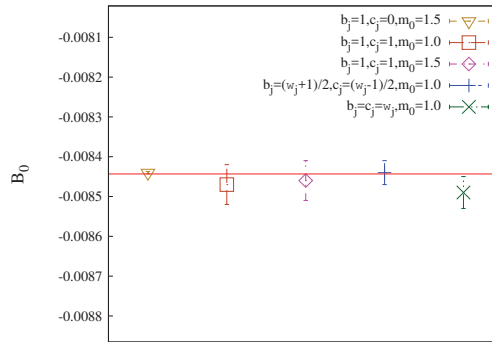
Figure 6.17 show the best fit results of B_0 for the MDWF with $N_5 = 16$ and the expectation value, $B_0 \simeq -0.00844343 \dots$. Data are obtained from Tabs. 6.6-6.10. I find that values of B_0 for MDWF are consistent with the expectation value.

Table 6.9: The optimal Shamir DWF with $m_0 = 1.0$.

N_5	8	16	∞
Fit range	$38 \leq L/a \leq 80$	$16 \leq L/a \leq 48$	-
A_0	-0.00085(30)	0.00110(16)	0.0010886(51)
B_0	-0.008299(50)	-0.00844(3)	0.00844343
A_1	0.1269(55)	0.0227(11)	-
B_1	-0.0386(28)	-0.0020(8)	-
$\chi^2/\text{d.o.f}$	3.46×10^{-7}	6.08×10^{-7}	-

 Table 6.10: The optimal Chiu DWF with $m_0 = 1.0$.

N_5	8	16	32	∞
Fit range	$32 \leq L/a \leq 72$	$34 \leq L/a \leq 72$	$32 \leq L/a \leq 48$	-
A_0	0.01033(94)	0.01114(3)	0.010851(12)	0.01118458(16)
B_0	-0.00835(16)	-0.00849(4)	-0.008389(2)	-0.00844343
A_1	-0.132(14)	0.037(4)	0.01564(14)	-
B_1	0.0623(76)	-0.004(2)	-0.00172(8)	-
$\chi^2/\text{d.o.f}$	1.40×10^{-6}	2.91×10^{-7}	1.74×10^{-9}	-


 Figure 6.17: The best fit results of B_0 for the MDWF with $N_5 = 16$. Data are used in Tabs. 6.6-6.10.

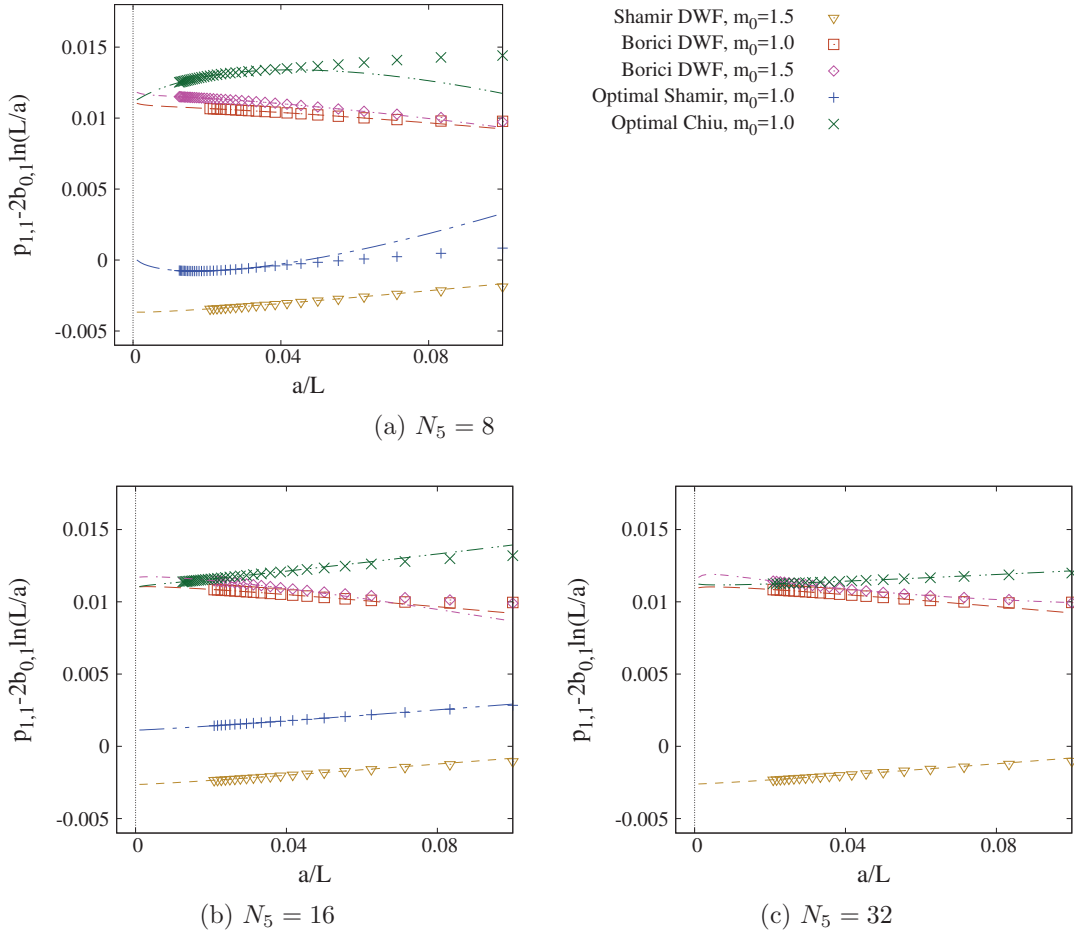


Figure 6.18: Lattice cutoff dependence of $p_{1,1} - 2b_{0,1} \ln a/L$. The lines represent the fitting function in Eq 6.3.3.

Figure 6.18 shows the one-loop coefficient, $p_{1,1} + (1/12\pi^2) \ln(L/a)$, as a function of a/L . The lines in these figures indicate the fitting results, and the parameters obtained by the fitting analysis are summarized in Tabs. 6.6-6.10.

From these data, it is apparent that the $O(a)$ error associated with the term B_1 is large for the optimal Shamir (plus sign symbols) and the optimal Chiu (cross symbols) DWFs at small values of N_5 , and that this error is reduced as N_5 becomes larger. I confirmed that the stability of B_0 over the fitting range was within 10%, except for the optimal Shamir and Chiu DWFs, at $N_5 = 8$. These DWFs exhibited a 20% deviation from the theoretical value, $2b_{0,1}$, for the fitted result, B_0 .

The consistency of A_0 was subsequently assessed by fitting $p_{1,1}$ as a function of Eq. (6.3.2) in the cases of $n = 1, 2$ and 3 with a fixed $B_0 = 2b_{0,1}$. The fitting results for A_0 are summarized in Table 6.11, in which the data in the column labeled $N_5 = \infty$ represent theoretical values based on consistency with the universality argument.

Table 6.11: Fitting results for A_0 .

Operator	m_0	$N_5 = 8$	$N_5 = 16$	$N_5 = 32$	$N_5 = \infty$
Optimal Shamir	1.0	-0.00100(18)	0.001076(15)	-	0.0010886(51)
Shamir	1.5	-0.00373594(6)	-0.0026696(16)	-0.002634(2)	-0.0026362(33)
Optimal Chiu	1.0	-	0.01103(15)	0.0111661(18)	0.01118458(16)
Boriçi	1.0	0.010952(9)	0.01116(3)	0.01116(4)	0.01118458(16)
Boriçi	1.5	0.011679(5)	0.01184(15)	0.01181(4)	0.01191070(16)

A_0 values could not be determined for the optimal Chiu DWF with $N_5 = 8$ because of the instability of the fitting results, although the values for A_0 in Table 6.11 agree with the expected values at sufficiently large N_5 values. I conclude that the MDWF must satisfy the universality argument up to the one-loop level at $N_5 = \infty$.

In order to investigate the $O(a)$ error, I analyzed A_1 and B_1 by fitting $p_{1,1}$ using the functions introduced in the determination of A_0 . In this analysis, I set the coefficients A_0 and B_0 to the theoretical constants at $N_5 = \infty$. Table 6.12 shows the fitting results for B_1 .

Table 6.12: Fitting results for B_1 .

Operator	m_0	N_5	16	32
Optimal Shamir	1.0		-0.00115(3)	-
Shamir	1.5		-	-0.0014(2)
Optimal Chiu	1.0		-0.0080(7)	-0.00490(3)
Boriçi	1.0		0.00116(6)	0.00112(4)
Boriçi	1.5		0.0041(13)	0.0038(9)

The systematic error in the results for B_1 was estimated using the same method as that for A_0 . B_1 for the Shamir DWF with $m_0 = 1.5$ and $N_5 = 16$ was omitted due to the instability of the fitting results when changing the fitting range. B_1 became smaller as N_5 was increased, demonstrating that lattice chiral symmetry of the MDWF was restored.

In the case of $B_1 \simeq 0$, I fitted A_1 using the equation,

$$p_{1,1}(a/L) - A_0 - 2b_{0,1} \ln(L/a) = A_1 \frac{a}{L} + (A_2 + B_2 \ln(L/a)) \left(\frac{a}{L}\right)^2. \quad (6.3.4)$$

as a function of a/L . The coefficients A_1, A_2 , and B_2 are free parameters and A_0 is the universal value for the MDWFs. Table 6.13 shows the fitting results for A_1 .

Table 6.13: Fitting results for A_1 with B_0 set at $-1/(12\pi^2)$ and A_0 set at the universal value at $N_5 = \infty$.

Operator	m_0	N_5	A_1
Optimal Shamir	1.0	16	0.0144(3)
Shamir	1.5	32	0.01409(11)
Boriçi	1.0	32	-0.0175(4)

6.3.2 The cutoff error for the step scaling function

To investigate the discretization error in the lattice step scaling function, I investigated the cutoff dependence and the discrepancy of the step scaling function in continuum theory. For the one-loop investigation in the lattice field theory, the $O(a)$ error of the SSF can be removed by tuning A_1 . The discretization error of the lattice SSF at the one-loop level is expressed by

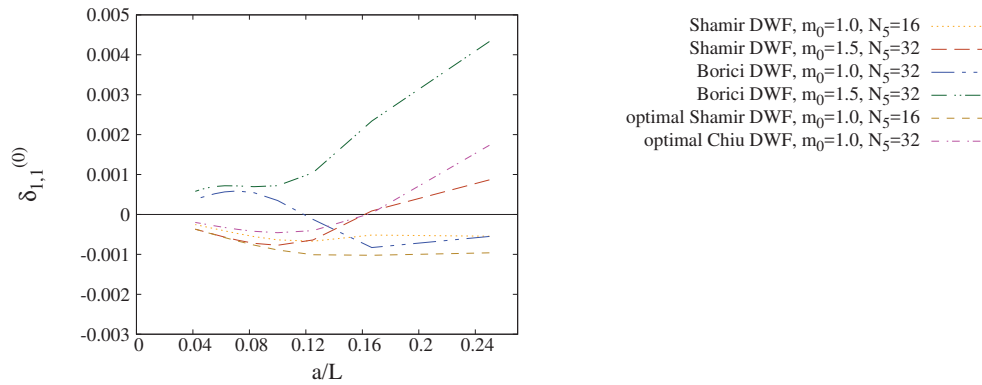
$$\delta_{1,1}^{(0)} = p_{1,1}(sL/a) - p_{1,1}(L/a) - 2b_{0,1} \ln s, \quad (6.3.5a)$$

$$\delta_{1,1}^{(1)} = p_{1,1}(sL/a) - p_{1,1}(L/a) - 2b_{0,1} \ln s + a/Lc_t, \quad (6.3.5b)$$

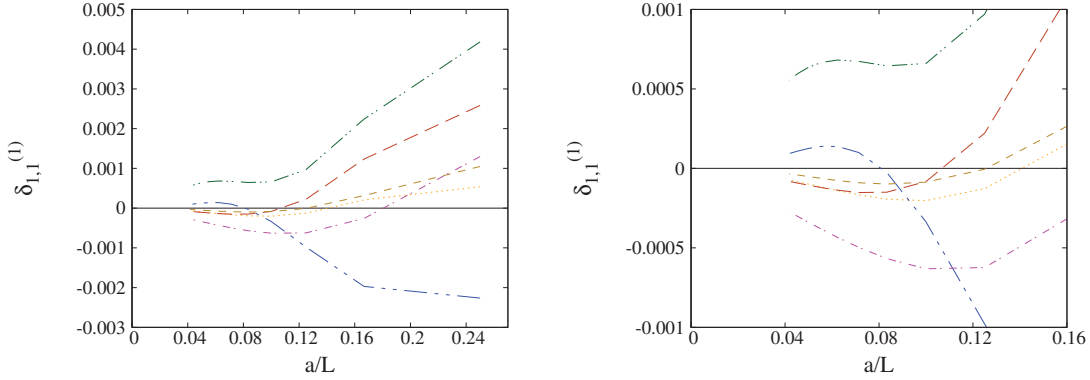
where s is a scaling factor and c_t is the coefficient of the counter term of the gluonic field. By adjusting the coefficient c_t to

$$c_t = \frac{A_1}{2}, \quad (6.3.6)$$

one can remove the $O(a)$ error from the term with A_1 in the SSF.


 Figure 6.19: Dependence of $\delta_{1,1}^{(0)}$ on lattice cutoff.

Figs. 6.19 and 6.20 show the lattice cutoff dependence of $\delta_{1,1}^{(0)}$ and $\delta_{1,1}^{(1)}$ respectively. For comparison, I also show $\delta_{1,1}$ values calculated from the DWF operator [41] in Figs. 6.19 and 6.20 (labeled Shamir DWF, $m_0 = 1.0, N_5 = 16$). From figure 6.19, it is evident that the magnitude of the lattice cutoff error, $\delta_{1,1}^{(0)}$, is similar to that associated with the MDWFs

Figure 6.20: Dependence of $\delta_{1,1}^{(1)}$ on lattice cutoff.

compared with the Shamir DWF. The magnitude of $\delta_{1,1}^{(1)}$ is modified by the $O(a)$ improvement with regard to A_1 , as seen in figure 6.20; $\delta_{1,1}^{(1)}$ is large in the large cutoff region, but it is very small in the small cutoff region for all operators. Although $\delta_{1,1}^{(1)}$ is larger than $\delta_{1,1}^{(0)}$ in the region $a/L \geq 0.1$ for the Shamir DWF with $(m_0, N_5) = (1.5, 32)$ and for the Boriçi DWF with $(m_0, N_5) = (1.0, 32)$, this value decreases with decreasing a/L .

I examine the consistency of the running coupling constant in the SF scheme with the MDWF at the one-loop level in Section 6.3, and discuss the consistency of the perturbative coefficients A_0 and B_0 . Based on the validation of the universality argument with the operator and the propagator at the tree-level in Sections 6.1 and 6.2, I conclude that the MDWF with the SF boundary term as proposed in this thesis is consistent with the proper SF theory.

Chapter 7

Summary and Outlook

Recent research regarding lattice quantum chromodynamics (LQCD) requires renormalization constants calculated using a non-perturbative renormalization scheme with the lattice chiral fermion. Lattice fermions as defined in the lattice field theory cannot correctly express the chiral symmetry, but this problem can be avoided thanks to the Ginsparg-Wilson (GW) relation. The GW relation is the alternative realization of chiral symmetry in lattice field theory, and lattice fermion that satisfies the GW relation is termed the lattice chiral fermion. Formalism and simulations of the lattice chiral fermion have been successfully performed, and the Möbius domain wall fermion (MDWF) is one such lattice chiral fermion. Several renormalization schemes are available for LQCD simulations, but there are few schemes that are applicable to non-perturbative renormalization on the lattice. The Schrödinger functional scheme is one possible non-perturbative renormalization approach, and has been successfully applied to lattice fermions without lattice chiral symmetry. Although applying the SF scheme to lattice chiral fermions is very helpful in the case of non-perturbative simulations, the temporal boundary condition imposed by the SF scheme is not compatible with lattice chiral fermions in a naive manner. To solve this problem, certain conditions are necessary for the lattice chiral fermion operator, based on the symmetries that the operator should possess.

In the work reported herein, I constructed an SF scheme for the MDWF and confirmed consistency with the continuum SF theory up to the one-loop level. The construction of the MDWF operator in the SF scheme involved imposing five-dimensional index symmetry on the MDWF. This modified the sign approximation function to allow determination of the MDWF parameters. The accuracy of the modified sign approximation function is somewhat lower than that of the original, but both exhibit similar levels of precision. A minimized fifth-dimensional lattice size was associated with explicit breaking of the lattice chiral symmetry, and operator renormalization as well as a mass shift in the effective four-dimensional operator with the MDWF at the tree-level were observed.

The properties of the MDWF operator were examined following tree-level renormalization, based on the unitarity condition and violation of the GW relation. The MDWF operator with the SF boundary term does not satisfy the unitarity condition obeying for the sign function due to the SF boundary condition. And the violation of the GW relation was retained only at the temporal boundary. I investigated the lowest eigenvalues, propagator and correlation

functions associated with the MDWF operator as a consistency check at the tree-level.

The lattice propagator in bulk time slices was found to be consistent with the continuum propagator at the continuum limit, while the lattice propagator at the temporal boundary exhibited a constant deviation at the continuum limit. This behavior required constant renormalization on the boundary field at the tree-level. I discussed the possibility of boundary operator renormalization and the consistency in terms of the field theoretical requirements. Having observed the consistency of the MDWF with the SF boundary condition at the tree-level, I also calculated the fermionic part of the one-loop beta function. The proposed MDWF with the SF boundary condition evidently reproduces the one-loop beta function together with the one-loop universal relation between the SF and $\overline{\text{MS}}$ schemes as $N_f \rightarrow \infty$. I also investigated the lattice artifacts resulting from the step-scaling function with the MDWF based on comparison those with artifacts resulting from Wilson-type fermions, and found that the size of the cutoff error is similar to that obtained with Wilson-type fermions. Based on these observations, the boundary operator introduced for the MDWF in this work to realize the SF scheme is evidently valid at least up to the one-loop level. Future work will involve studying the MDWF in the SF scheme, working in the non-perturbative domain. As an example, the step scaling function for the running coupling at higher and lower renormalization scales and the step scaling function with the MDWF should coincide with the known step-scaling function at the continuum limit.

Once the SF scheme with the MDWF is validated non-perturbatively, the SF scheme could be an attractive renormalization scheme for the study of hadron physics and elementary particle physics based on lattice QCD involving lattice chiral fermions. As an example, the Cabibbo-Kobayashi-Maskawa (CKM) matrix, which describes the quark mixing effect in the weak interaction, is a key observable in the beyond standard model in elementary particle theory. The CKM matrix describes not only the mixing structure but also the mass hierarchy of the quarks in the standard model. In this approach, the numerical values are extracted from the experimental hadron decay data by combining theoretical hadron matrix elements. The hadron matrix elements involve the chiral symmetry because of the weak interaction structure. Therefore, elements with chiral symmetry should be evaluated non-perturbatively with LQCD using the lattice chiral fermion so as to ensure a high level of precision. In this regard, the MDWF with the SF could help evaluate the precision of the hadron matrix elements, because the MDWF reduces the computational cost and the SF scheme is highly compatible with the $\overline{\text{MS}}$ scheme.

Acknowledgments

I am grateful to my supervisor, Ken-Ichi Ishikawa, for many helpful discussions regarding theoretical developments in this field and techniques of computer simulations. I would like to thank Professor Motoo Sekiguchi of the Department of Mathematics and Science, School of Science and Engineering, Kokushikan University, for acting as a sub-chief examiner of my doctoral dissertation. I also wish to thank Professor Yasushi Kojima for serving as a sub-chief examiner and for acting as the master examiner of my master's thesis. I am grateful to Professor Tomohiro Inagaki for examining my doctoral dissertation as a sub-chief examiner and for providing me with the opportunity to attend an international conference. Assistant Professor Shinji Takeda from the Institute for Theoretical Physics, Kanazawa University, provided useful computational advice and discussions regarding the behavior at the continuum limit of the DWF propagator with the SF scheme. This advice was crucial to the success of my research. Dr. Takayuki Miyagi of Center for Nuclear Study, the University of Tokyo gave me comments on the explanation of the study overview. He also gave me advice on the presentation related to this research. I am very thank to him. Finally, I wish to thank the members of the Theoretical Particle Physics group and Professor Masanori Okawa for giving me the opportunity to study LQCD from my master's work.

The numerical calculations in this work were performed during workstations at the Institute for Nonlinear Sciences and Applied Mathematics (INSAM) at Hiroshima University and using the FUJITSU PRIMERGY CX400 (Tatara system) at the Research Institute for Information Technology at Kyushu University. This work was supported by JSPS KAKENHI grants (numbers 24540276 and 16K05326) and as a project under the Core of Research for the Energetic Universe (CORE-U) program at Hiroshima University.

Appendix A

Notations

In this appendix, I explain the notations used in this thesis. μ and ν are the Lorentz indices and go from 1 to 4 in Euclidean space-time. γ_μ is the Euclidean Dirac gamma matrix that satisfies

$$\gamma_\mu^\dagger = \gamma_\mu, \quad \{\gamma_\mu, \gamma_\nu\} = 2\delta_{\mu,\nu}, \quad \gamma_5 \equiv \gamma_1\gamma_2\gamma_3\gamma_4. \quad (\text{A.0.1})$$

P_\pm and $P_{L/R}$ are the time-shift and chiral projection operators, respectively, written as

$$P_\pm = \frac{1 \pm \gamma_4}{2}, \quad P_{L/R} = \frac{1 \mp \gamma_5}{2}. \quad (\text{A.0.2})$$

For the five-dimensional space, I define various matrices and present the case of $N_5 = 6$ as an example. \mathcal{R} is defined as

$$\mathcal{R} = (\delta_{n_s, N_5 - m_s + 1}) = \begin{pmatrix} 0 & 0 & 0 & 0 & 0 & 1 \\ 0 & 0 & 0 & 0 & 1 & 0 \\ 0 & 0 & 0 & 1 & 0 & 0 \\ 0 & 0 & 1 & 0 & 0 & 0 \\ 0 & 1 & 0 & 0 & 0 & 0 \\ 1 & 0 & 0 & 0 & 0 & 0 \end{pmatrix}, \quad (\text{A.0.3})$$

and the chiral transform operator is

$$\Gamma = \begin{pmatrix} -1 & 0 & 0 & 0 & 0 & 0 \\ 0 & -1 & 0 & 0 & 0 & 0 \\ 0 & 0 & -1 & 0 & 0 & 0 \\ 0 & 0 & 0 & 1 & 0 & 0 \\ 0 & 0 & 0 & 0 & 1 & 0 \\ 0 & 0 & 0 & 0 & 0 & 1 \end{pmatrix}. \quad (\text{A.0.4})$$

Appendix B

Zolotarev sign approximation

Various sign function approximation methods are available, and these involve formulate lattice chiral fermions such as the overlap fermion. The Zolotarev sign function approximation is originally introduced for the overlap fermions to explicitly construct the sign function of matrices numerically and Chiu formulated the DWF with a Boriçi type setting of the Möbius parameter by Refs. [63, 71]. In this appendix, I introduce a means of obtaining ω_j via the Zolotarev sign function approximation and show the eigenvalue range for the kernel operators \mathcal{H}_ω used in the MDWF with the SF boundary condition.

ω_j is defined by the Zolotarev sign function approximation as

$$\omega_j = \frac{1}{\lambda_{\min}} \sqrt{1 - \kappa'^2 \text{sn}^2(v_i; \kappa')}, \quad (\text{B.0.1})$$

where $\text{sn}(v_i; \kappa')$ is the Jaccobi's elliptic function, and v_i and κ' is written as

$$\kappa' = 1 - \lambda_{\min}^2 / \lambda_{\max}^2, \quad (\text{B.0.2})$$

$$v_i = (-1)^{i-1} J \text{sn}^{-1} \left(\sqrt{\frac{1+3\lambda}{(1+\lambda)^3}}; \sqrt{1-\lambda^2} \right) + \left[\frac{i}{2} \right] \frac{2K'}{N_5}. \quad (\text{B.0.3})$$

J and λ are defined as

$$\lambda = \prod_{j=1}^{N_5} \frac{\Theta^2\left(\frac{2iK'}{N_5}; \kappa'\right)}{\Theta^2\left(\frac{(2i-1)K'}{N_5}; \kappa\right)}, \quad (\text{B.0.4})$$

$$J = \prod_{j=1}^{N_5/2} \frac{\Theta^2\left(\frac{(2i-1)K'}{N_5}; \kappa\right)}{\Theta^2\left(\frac{2iK'}{N_5}; \kappa'\right)}, \quad (\text{B.0.5})$$

where K' is the complete elliptic integral of the first kind expansion for κ' and Θ is the elliptic theta function. λ_{\min} and λ_{\max} are the minimum and maximum eigenvalues of the absolute value of the kernel operator, respectively, written as

$$\lambda_{\min} \equiv \min |\mathcal{H}_\omega|, \quad (\text{B.0.6})$$

$$\lambda_{\max} \equiv \max |\mathcal{H}_\omega|. \quad (\text{B.0.7})$$

We can see that the period of the elliptic function $\text{sn}(v_i; \kappa')$ depends on N_5 from Eqs. (B.0.4) and (B.0.5).

The matrix function, $U(\mathcal{H}_\omega)$ in Eq. (3.2.5) is described using ω_j as

$$U(\mathcal{H}_\omega) = R_{N_5}(\mathcal{H}_\omega) = \frac{\prod_{j=1}^{N_5} (1 + \omega_j \mathcal{H}_\omega) - \prod_{j=1}^{N_5} (1 - \omega_j \mathcal{H}_\omega)}{\prod_{j=1}^{N_5} (1 + \omega_j \mathcal{H}_\omega) + \prod_{j=1}^{N_5} (1 - \omega_j \mathcal{H}_\omega)}. \quad (\text{B.0.8})$$

When N_5 is sufficiently large, $U(\mathcal{H}_\omega)$ becomes the sign approximation which is the unitary matrix. At this point, we consider the error between the sign function and the Zolotarev sign function approximation, defined as

$$\delta_z^{N_5}(x) \equiv |\text{sgn}(x) - R_{N_5}(x)|. \quad (\text{B.0.9})$$

From Eqs. (B.0.1)-(B.0.3) and $\text{sn}(v_i; \kappa')^2 \leq 1$, values of ω_j are determined within range,

$$\frac{1}{\lambda_{\max}} < \omega_j < \frac{1}{\lambda_{\min}}. \quad (\text{B.0.10})$$

In order to determine w_j satisfying Eq. (B.0.10), we have to know the lowest and highest eigenvalues of \mathcal{H}_ω . I investigated the eigenvalues by varying the lattice size a/L and obtain the following estimates;

$$0.361893 \frac{a}{L} < a|\mathcal{H}_\omega| < 1.0 \quad (\theta = \frac{\pi}{5}, \text{ the Shamir kernel}), \quad (\text{B.0.11})$$

$$0.725254 \frac{a}{L} < a|\mathcal{H}_\omega| < 7.0 \quad (\theta = \frac{\pi}{5}, \text{ the overlap kernel}), \quad (\text{B.0.12})$$

$$0 \frac{a}{L} < a|\mathcal{H}_\omega| < 1.0 \quad (\theta = 0, \text{ the Shamir kernel}), \quad (\text{B.0.13})$$

$$0 \frac{a}{L} < a|\mathcal{H}_\omega| < 7.0 \quad (\theta = 0, \text{ the overlap kernel}). \quad (\text{B.0.14})$$

The Shamir kernel means the kernel operator made from the Shamir DWF in Eq. (3.2.10a) and the optimal Shamir DWF in Eq. (3.2.10c). *The overlap kernel* means the Boriçi DWF in Eq. (3.2.10b) and the optimal Boriçi DWF in Eq. (3.2.10d). From the above, the unitary function $U(\mathcal{H}_\omega)$ depends on a/L and N_5 . As seen from the lower boundary, the lowest eigenvalue becomes zero in the continuum limit. This means that the upper range in Eq. (B.0.10) becomes infinite resulting $N_5 \rightarrow \infty$ to keep the accuracy of the approximation Eq. (B.0.9) at a constant. Inversely saying, with w_j determined with a fixed $\lambda_{\min/\max}$ and a fixed N_5 , the accuracy of the approximation becomes worse and the approximation suddenly breakdowns when the eigenvalues spills out from the approximation range in taking the continuum limit.

Bibliography

- [1] H. Yukawa, Proc. Phys. Math. Soc. Jap. **17** (1935) 48 [Prog. Theor. Phys. Suppl. **1** 1].
- [2] M. Gell-Mann, Phys. Lett. **8**, 214 (1964).
- [3] G. Zweig, Developments in the Quark Theory of Hadrons, Volume 1. Edited by D. Lichtenberg and S. Rosen. pp. 22-101.
- [4] J. D. Bjorken, Phys. Rev. **179** (1969) 1547.
- [5] C. N. Yang and R. L. Mills, Phys. Rev. **96**, 191 (1954).
- [6] G. 't Hooft, Nucl. Phys. B **33**, 173 (1971).
- [7] G. 't Hooft, Nucl. Phys. B **35**, 167 (1971).
- [8] D. J. Gross and F. Wilczek, Phys. Rev. Lett. **30**, 1343 (1973).
- [9] H. D. Politzer, Phys. Rev. Lett. **30**, 1346 (1973).
- [10] M. Han and Y. Nambu, Phys. Rev. B **139**,1006 (1965).
- [11] K. G. Wilson, Phys. Rev. D **10**, 2445 (1974).
- [12] H. B. Nielsen and M. Ninomiya, Nucl. Phys. B **185**, 20 (1981)
- [13] Y. Nambu and G. Jona-Lasinio, Phys. Rev. **122**, 345, (1961).
- [14] Y. Nambu and G. Jona-Lasinio, Phys. Rev. **124**, issue 1, 246, (1961).
- [15] P. H. Ginsparg and K. G. Wilson, Phys. Rev. D **25**, 2649 (1982).
- [16] M. Luscher, Phys. Lett. B **428**, 342 (1998) [hep-lat/9802011].
- [17] D. B. Kaplan, Phys. Lett. B **288**, 342 (1992) [hep-lat/9206013].
- [18] V. Furman and Y. Shamir, Nucl. Phys. B **439**, 54 (1995) [hep-lat/9405004].
- [19] R. Narayanan and H. Neuberger, Phys. Lett. B **302**, 62 (1993) [hep-lat/9212019].
- [20] R. Narayanan and H. Neuberger, Phys. Rev. Lett. **71**, 3251 (1993) [hep-lat/9308011].

- [21] R. Narayanan and H. Neuberger, Nucl. Phys. B **412**, 574 (1994) [hep-lat/9307006].
- [22] R. C. Brower, H. Neff and K. Orginos, Nucl. Phys. Proc. Suppl. **140**, 686 (2005) [hep-lat/0409118].
- [23] R. C. Brower, H. Neff and K. Orginos, arXiv:1206.5214 [hep-lat].
- [24] S. Hashimoto, S. Aoki, G. Cossu, H. Fukaya, T. Kaneko, J. Noaki and P. A. Boyle, PoS LATTICE **2013**, 431 (2014).
- [25] G. Martinelli, S. Petrarca, C. T. Sachrajda and A. Vladikas, Phys. Lett. B **311**, 241 (1993) [Erratum-ibid. B **317**, 660 (1993)].
- [26] G. Martinelli, C. Pittori, C. T. Sachrajda, M. Testa and A. Vladikas, Nucl. Phys. B **445**, 81 (1995) [hep-lat/9411010].
- [27] M. Lüscher, R. Narayanan, P. Weisz and U. Wolff, Nucl. Phys. B **384**, 168 (1992) [hep-lat/9207009].
- [28] S. Sint, Nucl. Phys. B **421**, 135 (1994) [hep-lat/9312079].
- [29] M. Lüscher, R. Sommer, P. Weisz and U. Wolff, Nucl. Phys. B **413**, 481 (1994) [hep-lat/9309005].
- [30] S. Sint, Nucl. Phys. B **451**, 416 (1995) [hep-lat/9504005].
- [31] M. Lüscher, JHEP **1008**, 071 (2010) [Erratum-ibid. **1403**, 092 (2014)] [arXiv:1006.4518 [hep-lat]].
- [32] M. Lüscher and P. Weisz, JHEP **1102**, 051 (2011) [arXiv:1101.0963 [hep-th]].
- [33] Z. Fodor, K. Holland, J. Kuti, D. Negradi and C. H. Wong, JHEP **1211**, 007 (2012) [arXiv:1208.1051 [hep-lat]].
- [34] P. Fritzsche and A. Ramos, JHEP **1310**, 008 (2013) [arXiv:1301.4388 [hep-lat]].
- [35] H. Suzuki, PTEP **2013**, 083B03 (2013) [arXiv:1304.0533 [hep-lat]].
- [36] M. Lüscher, JHEP **1304**, 123 (2013) [arXiv:1302.5246 [hep-lat]].
- [37] Y. Taniguchi, JHEP **0512**, 037 (2005) [hep-lat/0412024].
- [38] Y. Taniguchi, JHEP **0610**, 027 (2006) [hep-lat/0604002].
- [39] M. Lüscher, JHEP **0605**, 042 (2006) [hep-lat/0603029].
- [40] S. Takeda, Nucl. Phys. B **796**, 402 (2008) [arXiv:0712.1469 [hep-lat]].
- [41] S. Takeda, Phys. Rev. D **87**, no. 11, 114506 (2013) [arXiv:1010.3504 [hep-lat]].

- [42] M. Lüscher and P. Weisz, Nucl. Phys. B **479**, 429 (1996) [hep-lat/9606016].
- [43] M. Lüscher, S. Sint, R. Sommer, P. Weisz and U. Wolff, Nucl. Phys. B **491**, 323 (1997) [hep-lat/9609035].
- [44] M. Lüscher, S. Sint, R. Sommer and H. Wittig, Nucl. Phys. B **491**, 344 (1997) [hep-lat/9611015].
- [45] K. Jansen *et al.* [ALPHA Collaboration], Nucl. Phys. B **530**, 185 (1998) [Erratum-ibid. B **643**, 517 (2002)] [hep-lat/9803017].
- [46] S. Capitani *et al.* [ALPHA Collaboration], Nucl. Phys. B **544**, 669 (1999) [hep-lat/9810063].
- [47] S. Sint *et al.* [ALPHA Collaboration], Nucl. Phys. B **545**, 529 (1999) [hep-lat/9808013].
- [48] A. Bode *et al.* [ALPHA Collaboration], Phys. Lett. B **515**, 49 (2001) [hep-lat/0105003].
- [49] M. Della Morte *et al.* [ALPHA Collaboration], Nucl. Phys. B **713**, 378 (2005) [hep-lat/0411025].
- [50] M. Guagnelli *et al.* [ALPHA Collaboration], JHEP **0603**, 088 (2006) [hep-lat/0505002].
- [51] M. Della Morte *et al.* [ALPHA Collaboration], Nucl. Phys. B **729**, 117 (2005) [hep-lat/0507035].
- [52] P. Dimopoulos *et al.* [ALPHA Collaboration], JHEP **0805**, 065 (2008) [arXiv:0712.2429 [hep-lat]].
- [53] Y. Murakami and K. I. Ishikawa, PoS LATTICE **2014**, 331 (2014) [arXiv:1410.8335 [hep-lat]].
- [54] Y. Murakami and K. I. Ishikawa, PoS LATTICE **2015**, 308 (2016) [arXiv:1701.07139 [hep-lat]].
- [55] Y. Murakami and Ken-Ichi Ishikawa, “The simplified construction of the Schrödinger functional scheme with the Möbius domain wall fermions”, CONFERENCE PROCEEDINGS Modern Trends In Physics, Baku, Baku University Publishing House, 146-149 (2017).
- [56] Y. Murakami and K. I. Ishikawa, Int. J. Mod. Phys A, **33**, 1850012(2018).
- [57] S. Sint and R. Sommer, Nucl. Phys. B **465**, 71 (1996) [hep-lat/9508012].
- [58] Y. Kikukawa and T. Noguchi, hep-lat/9902022.
- [59] Y. Kikukawa, Nucl. Phys. B **584**, 511 (2000) [hep-lat/9912056].
- [60] A. Boriçi, Nucl. Phys. Proc. Suppl. **83** (2000) 771 [hep-lat/9909057].

-
- [61] A. Boriçi, in *Lattice Fermions and Structure of the Vacuum*, V. Mitrjushkin *et al.* (eds.), Springer 2000, [hep-lat/9912040].
- [62] A. Boriçi, in *QCD and numerical analysis III*, A. Boriçi *et al.* (eds.), Springer 2005, [hep-lat/0402035].
- [63] T. W. Chiu, *Phys. Rev. Lett.* **90**, 071601 (2003) [hep-lat/0209153].
- [64] S. Capitani, *PoS LAT 2007*, 066 (2007) [arXiv:0708.3281 [hep-lat]].
- [65] K. Symanzik, *Nucl. Phys. B* **226**, 205 (1983).
- [66] M. Luscher, S. Sint, R. Sommer and P. Weisz, *Nucl. Phys. B* **478** (1996) 365 [hep-lat/9605038].
- [67] Y. C. Chen and T. W. Chiu, *Phys. Lett. B* **738**, 55 (2014) [arXiv:1403.1683 [hep-lat]].
- [68] K. Ogawa *et al.* [TWQCD Collaboration], *PoS LAT 2009*, 033 (2009) [arXiv:0911.5532 [hep-lat]].
- [69] S. Sint, *Nucl. Phys. B* **847** (2011) 491 [arXiv:1008.4857 [hep-lat]].
- [70] S. Aoki and Y. Kuramashi, *Phys. Rev. D* **68** (2003) 034507 [hep-lat/0306008].
- [71] T. W. Chiu, T. H. Hsieh, C. H. Huang and T. R. Huang, *Phys. Rev. D* **66**, 114502 (2002) [hep-lat/0206007].